DOCTORAL DISSERTATION SERIES
Publication No.: 12,542

AUTHOR: George Breckenridge Beard, Ph. D., 1955
University of Michigan

TITLE: THE RADIOACTIVITIES OF Sm^{147} AND K^{40}

University Microfilms, Ann Arbor, Michigan

THE RADIOACTIVITIES OF Sm^{147} AND K^{40}

by

George Breckenridge Beard

A dissertation submitted in partial fulfillment
of the requirements for the degree of
Doctor of Philosophy in the
University of Michigan
1955

Committee in charge:

Associate Professor M.L. Wiedenbeck, Chairman
Professor H.R. Crane
Professor D.M. Dennison
Associate Professor W. Kaplan
Associate Professor R.W. Pidd

ABSTRACT

THE RADIOACTIVITIES OF Sm^{147} AND K^{40}

by George B. Beard

This thesis consists of two parts; a study of the alpha activity of the Sm^{147} isotope and an investigation of the beta activity of K^{40}.

The alpha activity of the Sm^{147} was measured using a proportional counter having 4π geometry. The sources were prepared by evaporating samarium chloride onto thin, aluminized zapon films with the total source thicknesses varying from .06 to .24 milligrams per cm^2. Both natural samarium and electromagnetically enriched samarium, which contained 78.35% Sm^{147}, were used. The amount of samarium present in each source was determined by means of a spectroscopic analysis. The measured activity of 719 $\pm$ 36 counts/sec-gm Sm^{147} corresponds to a half-life of $1.25 \pm .06 \times 10^{11}$ years.

The investigation of the energy spectrum of the alpha particles was carried out by measuring the alpha tracks produced in an Eastman NTA 25 micron nuclear plate after it was placed in contact with a thin evaporated source of the enriched samarium. The resulting histogram showed an energy spectrum that was nonoenergetic with an alpha particle energy of 2.11 $\pm$ .05 Mev.

This energy was used, along with an assumed nuclear radius (obtained from the alpha decay data for Gd^{148}), to calculate the expected activity of the Sm^{147}. The calculated activity was found to be

less than the measured activity by a factor of about one hundred. This difference cannot be readily explained. In order to get agreement between the two activities one would have to assume either a 6% increase in the measured energy up to a value of around 2.24 Mev or a 17% increase in the nuclear radius, or possibly some combination of smaller increases in both. Since the uncertainties in the energy and radius are much smaller than these values, it appears quite unlikely that they could account for all of the discrepancy between the activities.

As a possible explanation an approximate calculation was made to see if some nuclear deformation (specifically, that corresponding to a large positive quadrupole moment with a uniform nuclear charge distribution) could account for the difference. The results showed very qualitatively that one might expect such a nuclear deformation to increase the alpha activity to the right order of magnitude.

In the second part of the thesis the beta spectrum of K^{40} was investigated with the aid of a scintillation spectrometer. By using a comparitively large (31 grams) thallium activated KI crystal as the scintillation element it was hoped that the beta spectrum could be obtained free from distortion at low energies. Then the low energy region could be used to distinguish experimentally between the unique second and third-forbidden correction factors applied to the Fermi plot of the spectrum.

The observed beta spectrum was corrected for the following effects:

1) background,
2) K^{40} gamma rays,
3) resolution,
4) electron escape from the surface.

The corrected spectrum was then used to make the Fermi plots. Although the result was an improvement over previous work, it was found that both

correction factors linearized the Fermi plot equally well down to an energy of about 200 Kev. To distinguish between them one must find a way of measuring the spectrum free from distortion to even lower energies.

A As a check on the validity of the method the beta spectrum of K^{42} was measured in the region above 2Mev. When the unique first-forbidden correction factor was applied to the Fermi plot it was made linear in agreement with the theory and other experimental results.

By measuring the total activity of the KI crystal the beta activity of K^{40} was found to be $27.4 \pm .4$ particles per second per gram of natural potassium. This result agrees well with other measurements using a 4π geometry.

ACKNOWLEDGEMENTS

The author wishes to express his appreciation of the generous aid and encouragement given him by Associate Professor Marcellus L. Wiedenbeck during the course of this work.

He is grateful to the various other members of the Physics Department who have either directly or indirectly helped in the preparation of this thesis. The author wishes to especially thank Professor H.R. Crane for his continued interest, Professor G.E. Uhlenbeck and Associate Professor K.M. Case for stimulating discussions on the decay rate of Sm^{147}, as well as Mr. Stanley Derby and Dr. J.H. Enns for their assistance in carrying out the spectroscopic analysis.

TABLE OF CONTENTS

CHAPTER

INTRODUCTION 1

I. THE ALPHA ACTIVITY OF Sm^{147} 4

1. History 4
2. Description of Apparatus and Procedure 7
   a. Proportional counter. 7
   b. Preparation of sources. 9
   c. Spectroscopic analysis. 12
   d. Electronics 16
3. Activity Determination 16
4. Half-life Calculation 19
5. Energy Spectrum. 20

II. THEORY OF ALPHA DECAY 24

1. General Description. 24
2. Energy Considerations. 26
3. Theoretical Treatment. 28
   a. One body model. 28
   b. Many body model 31
   c. Penetration factor. 33
   d. Angular momentum of the alpha particle. 34

III. COMPARISON OF EXPERIMENTAL RESULTS WITH THE THEORY. . . . 36

IV. BETA ACTIVITY OF K^{40} AND K^{42}. 45

1. History of Beta Spectrum Measurements of K^{40} 45
2. Scintillation Spectrometer 48
3. K^{40} Beta Spectrum. 50
4. Corrections. 53
   a. Background. 53
   b. Gamma ray absorption. 53
   c. Resolution. 55
   d. Surface effect. 57
5. Measurement of the Total K^{40} Beta Activity 62
6. Beta Spectrum of K^{42} 64

TABLE OF CONTENTS (Concluded)

CHAPTER

V. THEORY OF BETA DECAY. 66

1. Selection Rules. 71
2. Shape of the Beta Spectrum 71

VI. APPLICATION OF THEORY TO EXPERIMENTAL RESULTS 73

1. Fermi Plot of K^{40}. 73
2. Fermi Plot of K^{42}. 75

REFERENCES. 79

LIST OF FIGURES

FIGURE		
1	Proportional Counter	8
2	Performance Test	10
3	Typical Counting Rate Curves	11
4	Half-life Extrapolation	18
5	Number of Tracks vs Range for Sm^{147}	21
6	Number of Tracks vs Range for Po^{210}	21
7	Complex Alpha Decay	25
8	Complex Alpha Decay (ThC' and RaC')	25
9	V(r) for Alpha Particle	30
10	Variation of log $(1/\lambda)$ with E	38
11	Variation of log $(1/\lambda)$ with R	39
12	Gamma Ray Spectrum of Co^{60}	49
13	Energy Calibration	51
14	Check for Multiple Counting	52
15	Estimated K^{40} Gamma Ray Spectrum	54
16	Observed N(E) for K^{40}	56
17	Corrected N(E) for K^{40}	61
18	Integral Counting Rate for K^{40}	63
19	Fermi Plots of K^{40}	74
20	Fermi Plots of K^{40}	76
21	Fermi Plots of K^{42}	78

LIST OF TABLES

TABLE

I. Naturally Occurring Radioactive Isotopes with $Z < 80$. . . .3

II. Sm^{147} Activity Measurements 6

III. Data for K^{40}. 60

INTRODUCTION

The decay of radioactive nuclei can be classified into four categories; alpha decay, beta decay, gamma emission and fission. Fission and alpha decay are closely related processes. In alpha decay particles identical with bare helium neclei are emitted, while in fission a nucleus will split into two more or less equal components. Beta decay, on the other hand, is somewhat more complex and can be divided into three subclasses; negative electron (β^-) decay, positive electron, or positron (β^+) decay, and K capture. As the names imply beta particles are identical to the corresponding negative and positive electrons. In K capture one of the orbital atomic electrons is captured by the nucleus and the name results from the fact that this happens most frequently to electrons in the K shell because of their greater proximity to the nucleus. Gamma emission takes place when a nucleus goes from an excited state to one of lower energy with the emission of a high energy photon. Usually a given isotope decays by one or two of these processes, but it sometimes happens that both alpha and beta decay as well as gamma emission take place.

Naturally occurring radioactive elements have long been known to exist and over the period of the last half century every element has been investigated for possible radioactivity. Of the lighter elements

with atomic number less than 80 only 10 have been shown to exhibit natural radioactivity. These are listed in Table I.

In this thesis the radioactivities of the naturally occurring Sm^{147} and K^{40} isotopes are investigated.

TABLE I

Naturally Occurring Radioactive Isotopes with Z < 80

Isotope	Isotopic Abundance(%)	Type of decay	E max (Mev)	Half-life (years)	Reference
$_{19}K^{40}$	.0119	Beta Gamma	1.33 1.46	1.29×10^9	--
$_{37}Rb^{87}$	27.85	Beta	.275	6.2×10^{10}	2
$_{49}In^{115}$	95.8	Beta	.63	6×10^{14}	1
$_{57}La^{138}$	.089	Beta Gamma	1.0 1.39 .81 .54	$\sim 7 \times 10^{10}$	1
$_{60}Nd^{144}$	23.9	Alpha	1.9	$\sim 1.5 \times 10^{15}$	3
$_{60}Nd^{150}$	5.6	Beta		$>10^{13}$	1
$_{62}Sm^{147}$	15.07	Alpha	2.12	1.25×10^{11}	--
$_{71}Lu^{176}$	2.60	Beta Gamma	.4 .270 .181 .089	7.5×10^{10}	1
$_{74}W^{(?)}$		Alpha	3.2	$\sim 6 \times 10^8$(calc)	4
$_{75}Re^{187}$	62.93	Beta	.043 .400	4×10^{12}	1

CHAPTER I

THE ALPHA ACTIVITY OF Sm^{147}

1. HISTORY

Among the 10 elements listed in Table I only samarium, wolfram, and neodymium emit alpha particles. The neodymium and wolfram activities have only recently been reported[3,4] while the alpha activity of samarium was discovered by Hevesy and Pahl[5] in 1932. It was not until eighteen years later that the activity was established as being due to the Sm^{147} isotope[6,7]. Since the discovery, various investigators have attempted to determine the half-life and energy spectrum of the emitted alphas. Table II summarizes their results with the half-lifes being corrected for the proper isotopic abundance of Sm^{147}.

In the early work by Hevesy, Pahl and Hosemann[8], Libby[9], and Hosemann[10], geiger counters were used to measure the activity. They were handicapped by the lack of modern electronic equipment and counting techniques and as a result their work can be considered as only approximately correct. Not only did they use poor geometry, but their sources were not thin and hence had large self-absorption.

Later investigations[11-14] were carried out using nuclear emulsions. In these cases a measured quantity of a samarium salt solution was absorbed by the emulsion of a nuclear plate and the subsequent

alpha tracks were observed. There were several major sources of error in this method. Probably the most important was the loss of some of the tracks from those Sm^{147} nuclei which were on or near the emulsion surface. Then there was the difficulty in defining the active area as well as the chance of missing tracks while scanning the plate. With track lengths of around 7 microns any tracks making angles of over 75 degrees with the plane of the emulsion would be so short that they might well be overlooked. Each of these errors would produce a lower recorded activity and it is interesting to note that the activity determinations by this method are lower than that measured in the present experiment. The nuclear emulsion method does have the advantage, though, of showing directly whether there are any of the more common longer range alpha emitters present as a source of contamination.

In view of the uncertainties in the previous investigations and the discrepancies among the results it was felt worthwhile to investigate the half-life using improved techniques and source materials. Both natural and electromagnetically enriched Sm were available. The natural Sm with 15.07% Sm^{147} (15) was about 98% pure Sm_2O_3 (16) and the enriched Sm with 78.35% Sm^{147} was over 99.6% pure Sm_2O_3 (17). Agreement using these different sources as well as proof of the absence of higher energy alpha particles due to contaminating elements would constitute good evidence for the validity of the final results. Therefore it was decided to make a new half-life determination and to investigate the energy spectrum using the enriched Sm.

TABLE II

Sm^{147} Activity Measurements

Observer	Year	Particles Observed	Range (cm in air NTP / μ in emulsion)	Half-life (years)
Hevesy and Pahl[5]	1932	1 alpha		
Hevesy, Pahl and Hosemann[8]	1933	1 alpha	1.13 cm	1.8×10^{11}
Mäder[12]	1934	1 alpha 1 proton	1.16 cm 1.37 cm	1.5×10^{11}
Libby[9]	1934	1 alpha	1.23 cm	$(9.5 \pm .8) \times 10^{10}$
Hosemann[10]	1936	1 alpha	1.13 cm	1.5×10^{11}
Taylor and Dabholker[11]	1936	1 alpha 1 longer range particle	1.13 cm	
Lattes and Cuer[14]	1946	1 alpha	$1.12 \pm .03$ cm	$(1.7 \pm .1) \times 10^{11}$
Keller and Mather[27]	1948	1 alpha	1.12 cm	
Haenny, Najar and Gailloud[29]	1949	1 alpha	$\sim 7.06 \mu$	
Bestenreiner and Broda[28]	1949	1 alpha		
Piccioto[13]	1949	1 alpha	$7.84 \pm .03 \mu$	$3.8 \pm .2 \times 10^{11}$
Jesse and Sadauskis[31]	1950		1.11 cm	
Stzeinsznaider[30]	1953	1 alpha	$\sim 7.15 \mu$	
Waldron, Schultz, and Kohman[3]	1954	1 alpha	7.1μ	

2. DESCRIPTION OF APPARATUS AND PROCEDURE

a. Proportional Counter

Since the alpha particles from Sm^{147} have such a short range, it is necessary to use thin sources to minimize self-absorption. Also, a large surface area is required to provide enough counts to give good statistics within reasonable counting times. In order to measure the counting rate directly and thus eliminate corrections due to backscattering and other results of poor geometry one needs to use a counter with 4 pi geometry. Such a counter, capable of using large, thin sources, has been developed by Sawyer and Wiedenbeck and described in detail by Sawyer in his thesis[18]. A sketch of the general features is given in Fig. 1. As can be seen from the figure it consists of two pancake type counters placed above and below the source with an arrangement whereby a blank film can be made to replace the source without disturbing the counter filling. In this way the background count can be measured under the same conditions as the Sm^{147} activity.

The counter was originally developed and tested to be used in the geiger region for the counting of beta particles from K^{40}. However, to count alpha particles one prefers to work in the proportional region since this greatly reduces the background. Consequently, it was necessary to establish that the counter would perform satisfactorily in the proportional region also.

The range of the Sm^{147} alphas is about 1.1 cm in air. To insure that all the energy would be expended either in the source or the counter gas the counter was filled with 20 cm of methane and 41 cm of argon. Then, after replacing the 20 mil tungsten central wires by

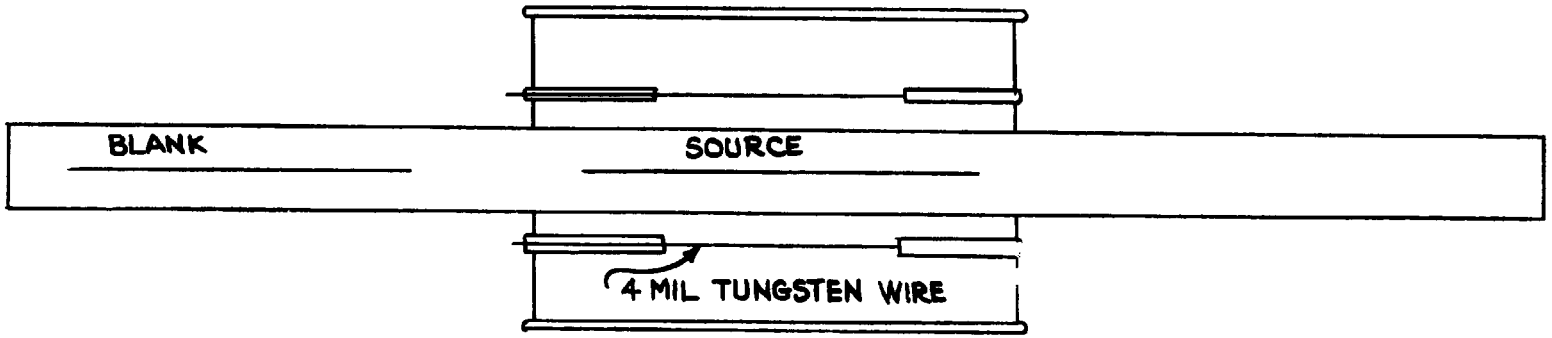


FIG. 1
PROPORTIONAL COUNTER

THE SOURCE AND BLANK ARE MOUNTED ON A SLIDING TRAY SO THAT EITHER CAN BE PLACED IN THE ACTIVE AREA WITHOUT DISTURBING COUNTER FILLING

SCALE: 1 CM. = 1 INCH

ones of 4 mil diameter, it was found that the counter performed well in the proportional region with the central wires at a potential of about 2500 volts. Figure 2 shows the result when a point source of Po^{210} alphas was moved across the counter along a diameter in one-half inch steps. The drop in the counting rate at the center occurred where the field became weaker[18]. The extent of the area of lower efficiency was inversely proportional to the operating voltage. For a further check the pulse height distribution of the polonium source was observed at several different positions. As expected, the resolution grew poorer when the point source was moved into the central region, changing from 20% to about 30%. After considering the magnitude and relative areas of lowered efficiency in the center and along the outside edge, the overall counter efficiency was taken to be 98%.

When the samarium sources were used the counter was stable with a plateau of about 100 volts. Figure 3 shows typical counting rate curves for a Sm source with the corresponding background.

b. Preparation of Sources

Two methods were tried for the preparation of thin sources. First, a water suspension of finely ground samarium oxide was sprayed onto an aluminized zapon film using a special atomizer which gave a very fine spray. Since the chemical composition of the oxide is fixed, this method had the advantage that the amount of Sm could be determined by merely weighing the source. However, it also had two major disadvantages which caused it to be abandoned. Although the oxide particles were fairly evenly dispersed, their size was still appreciable in comparison to the range of the alphas and resulted in

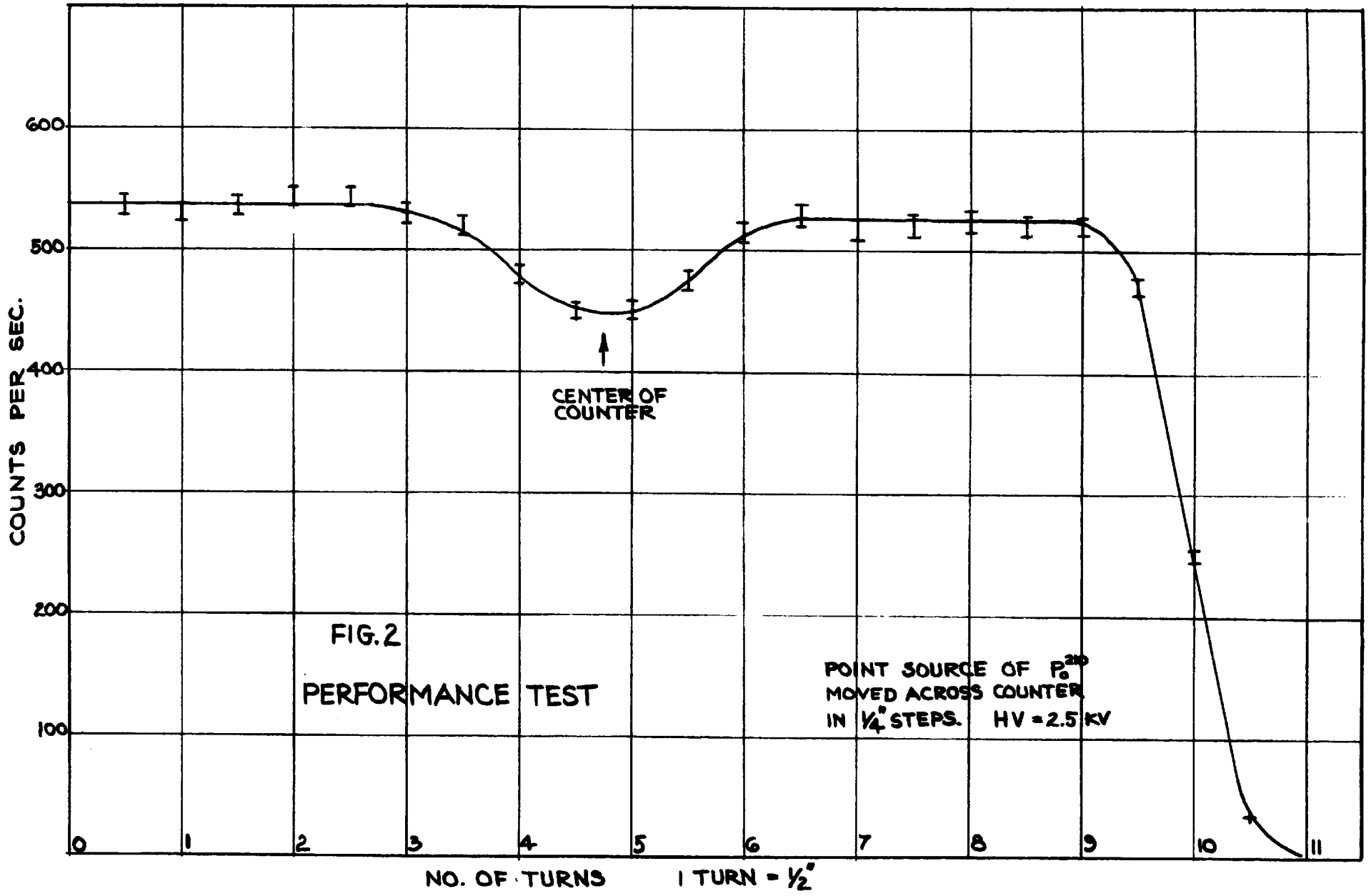


FIG. 2

PERFORMANCE TEST

POINT SOURCE OF Po^{210} MOVED ACROSS COUNTER IN ¼" STEPS. HV = 2.5 KV

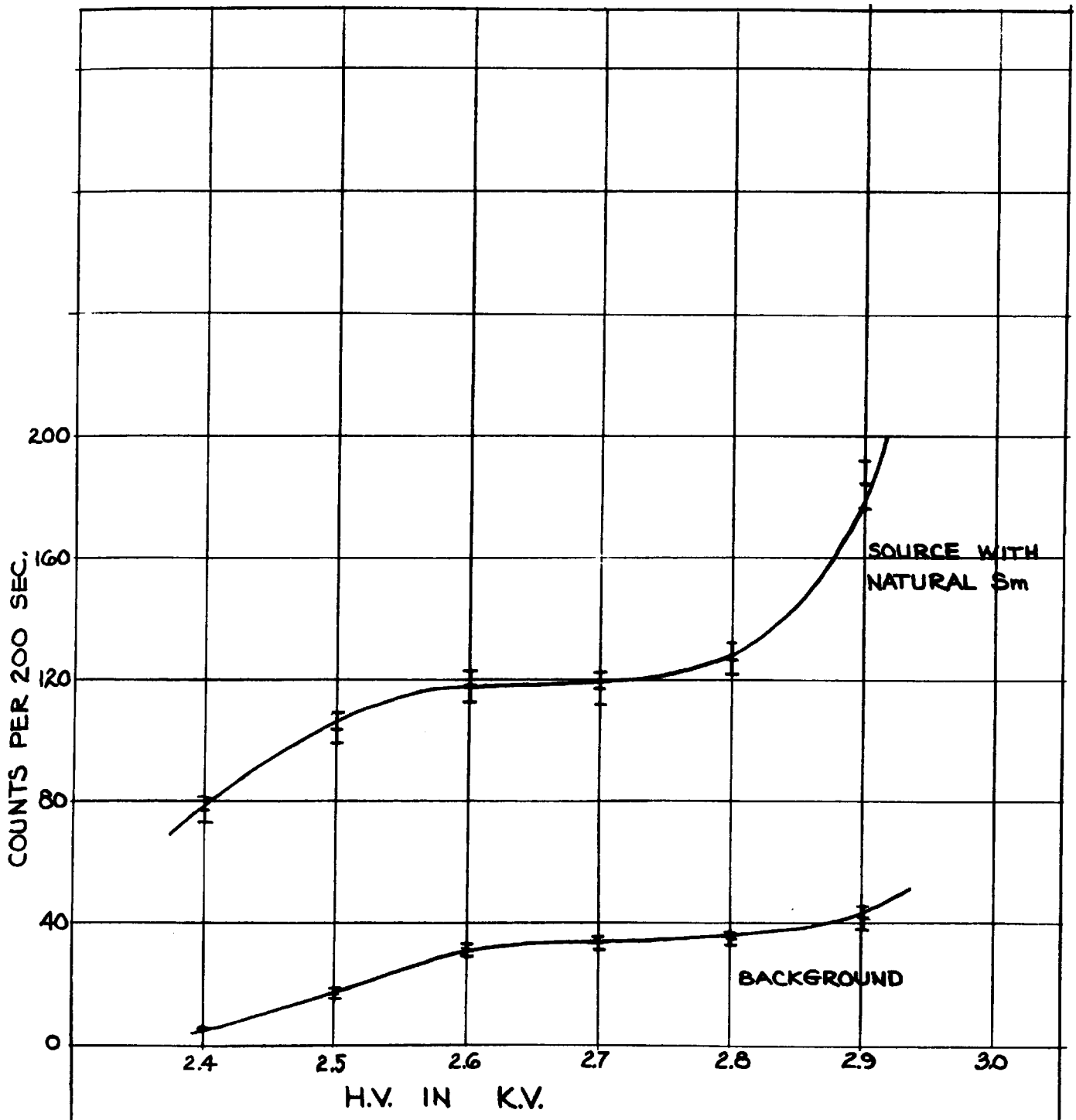


FIG. 3

TYPICAL COUNTING RATE CURVES

large self-absorption. Then, too, once dry the oxide particles did not adhere well to the zapon film and even with careful handling some would fall off making the amount of Sm change by as much as a few percent while the source was being used. This had the double effect of raising the background count as well as lowering the Sm^{147} counting rate.

The method chosen to overcome these difficulties was to prepare a source by evaporation in a vacuum. After a series of tests it was found that quite efficient evaporation could be achieved using samarium chloride placed in a molybdenum crucible. (Molybdenum was used because samarium tends to form intermetallic compounds with some of the other more commonly used metals[19].) Thus, by evaporating a layer of aluminum onto a zapon film followed by a similarly deposited layer of samarium chloride, a thin, microscopically uniform source could be prepared. The samarium chloride was made by treating the oxide with HCl and then evaporating the solution to dryness in an electric oven at about 60°C. Higher temperatures of around 100°C cause the undesireable oxychloride to be formed.

In the half-life determination the total average source thicknesses varied from .06 to .24 milligrams per cm^2. Since the samarium alpha particles have a range of 1.7 mg/cm^2, the sources would not be expected to have a large self-absorption. This is substantiated by the observation that an increase in the source thickness by a factor of four only decreased the counting rate by about 15%.

c. Spectroscopic Analysis

Although the sources prepared in this manner were thin and microscopically uniform, a major difficulty was introduced. It was due

to the fact that when samarium chloride is evaporated there is some question as to its final chemical composition.[19,20] It is possible that some of the samarium chloride, ($SmCl_3$), goes over into samarous chloride, ($SmCl_2$), or it may pick up waters of hydration to become $SmCl_3 \cdot 6H_2O$. Consequently, it was necessary to make a quantitative analysis for the amount of Sm present in each source. Considering that only a few milligrams of samarium were to be measured in each case, a quantitative chemical analysis would have been virtually impossible and so a spectroscopic analysis was decided upon.

In setting up the spectroscopic analysis a series of trial runs showed that the Cu line at 2961.2 A°. could be used as an internal control with the Sm line at 3216.8 A°. A large quantity of 10% HCl stock solution was prepared and enough copper sulphate was added to make a Cu concentration of 2 mg/cc. Then several standards were made with known concentrations of samarium. A quantity of the Sm_2O_3 was weighed and dissolved in a measured volume of the stock solution to make the most concentrated standard. The others were then prepared by successive dilutions. Several independent standards were also made as further checks. The unknown samples were prepared by immersing the zapon films in a measured amount of stock solution until both the aluminum and samarium chloride had completely dissolved.

Each of the solutions was diluted by adding an equal volume of concentrated sulfuric acid and a porus carbon cup was used to control the rate of flow of solution into the spark source of a large Littrow prism spectrograph. The addition of the sulfuric acid, along

with a 20 second pre-exposure time with the regular 40 second exposure interval, helped to improve the reproducibility of the runs. At the end of each run before being discarded the porus cup was examined to see that it had neither run dry nor boiled over. Any deviation from the norm caused the run to be disregarded.

The spectra were recorded on a No. 33 photographic plate. After development a microphotometer was used to compare the relative densities of the two Cu and Sm lines in each spectrum. The spectrum of iron was also included on each plate and several of the iron lines were used for calibration. In the analysis of each sample a half dozen runs were recorded on the photographic plate along with spectra from two of the standards. A good estimate of the amount of Sm in a source could be obtained by weighing and by proper choices of the amounts of stock solutions used the unknown concentrations were kept between .125 and .250 mg/cc. This region gave line densities well above the background while providing a fair amount of solution to be analyzed even when the amount of Sm on the source was as little as a milligram. All quantities involved in making the standards and unknown solutions were measured to an accuracy greater than 1%.

The average of the unknown runs was taken to be the amount of Sm in the sample and the uncertainty was estimated from the reproducibility of the separate runs. In some instances, where there was enough of the unknown sample, two separate plates were run as a further check on the accuracy. The accuracy of the best runs was judged to be within 3% by comparison with similar trials using the standards.

This procedure worked well with the natural samarium oxide. However, upon going to the enriched Sm it was discovered that the Sm line became too weak to use. A detailed comparison with the spectra of the possible contaminating elements revealed that the added intensity of the Sm line was due to the yttrium line at 3216.7 A°. From the data on the purity of the Sm_2O_3 and the relative intensities of the two lines[21] such a large contribution from yttrium line was unexpected. However, since the chemistry of the two elements is so similar,[20] it was concluded that the relative abundance of the yttrium impurity would not be significantly changed during the evaporation procedure and hence the spectroscopic analysis would be valid as long as the standards and unknowns were made from the same source of samarium.

The unexpectedly large contribution of the yttrium line indicates that the claim of 98% purity for the natural Sm_2O_3 may have been a bit optimistic and this conclusion is strengthened by the experimental results. The counting rates for the natural samarium all fell slightly below the corresponding values for the enriched Sm runs, but the average difference lies well within the overall estimated experimental error and gives good evidence for the accuracy of both spectroscopic analysis procedures.

Since the line at 3216.8 A° was not suitable for use with with the enriched Sm it was necessary to go to a new region of the spectrum to find a stronger line. A suitable line was found at 3609.5A° and the 3602.0 A° Cu line was used as the control. A new quantity of 10% HCl solution was prepared with 15 mg/cc of Cu and new standards were made containing enriched samarium oxide which was weighed

to an accuracy of better than 1% on a microbalance. Only one-third as much concentrated sulfuric acid was added to the solutions and the spectra were recorded on SA No. 1 photographic plates using a different Littrow prism spectrograph, but the general procedure was the same as had been carried out with the natural Sm. The somewhat larger uncertainties in the results are predominately due to the lesser quantities of the unknown solutions available which in turn were caused by the smaller amounts of Sm in the sources.

d. Electronics

The circuitry involved in the operation of the counter was straightforward. A Higgenbotham[22] type high voltage supply was used to furnish the operating voltage. The output pulses from the counter were fed through a standard cathode follower pre-amplifier into a differential discriminator based on a design in Elmore and Sands.[23] In the regular runs the integral out pulses from the discriminator were used so that all pulses from the amplifier with an amplitude greater than six volts were passed on into a Nuclear Instrument Model 161 scalar with Mercury register.

3. ACTIVITY DETERMINATION

Using a blank film this arrangement gave a background counting rate of about 0.16 counts per second while the counting rates of all but the weakest sources were more than a factor of two greater. The positions of the blank and sources were interchanged at times to insure against spurious counts caused by possible contamination of one

section of the sliding tray and not the other. Several different blanks were used in the course of the experiment.

During a run alternate readings were taken of the source and background counting rates until the Sm counting rate could be determined with a standard error of less than 2% for those sources containing natural Sm and about 1% for those with the enriched Sm.

For the determination of the actual counting rate the results of five runs with natural Sm and six runs with enriched Sm were used. Three other runs using a second supply of natural samarium chloride as a starting material were found to give results consistently about 25% too high. However, in the spectroscopic analysis the standards were those made using the natural Sm_2O_3 and, since the results therefore depended on the relative amounts of yttrium impurity present, it is not surprising that consistent results were not obtained. In an attempt to utilize thinner zapon films a thin wire was stretched across the center of two source rings and blank, but these results were also discarded when it became apparent that after the addition of a wire the background counting rate increased significantly. It is not known whether the increase in the background counting rate was actually due to the addition of the wire or whether the rings had somehow become contaminated. It was definitely established, though, that the rings gave a background counting rate which was about 30% above the normal value.

Figure 4 shows a graph of the counting rate per gram of Sm^{147} plotted against the total source thickness with the flags representing a combination of the statistical counting errors and the uncertainties in the analysis measurements. In most cases the counting error forms a negligible fraction of the total.

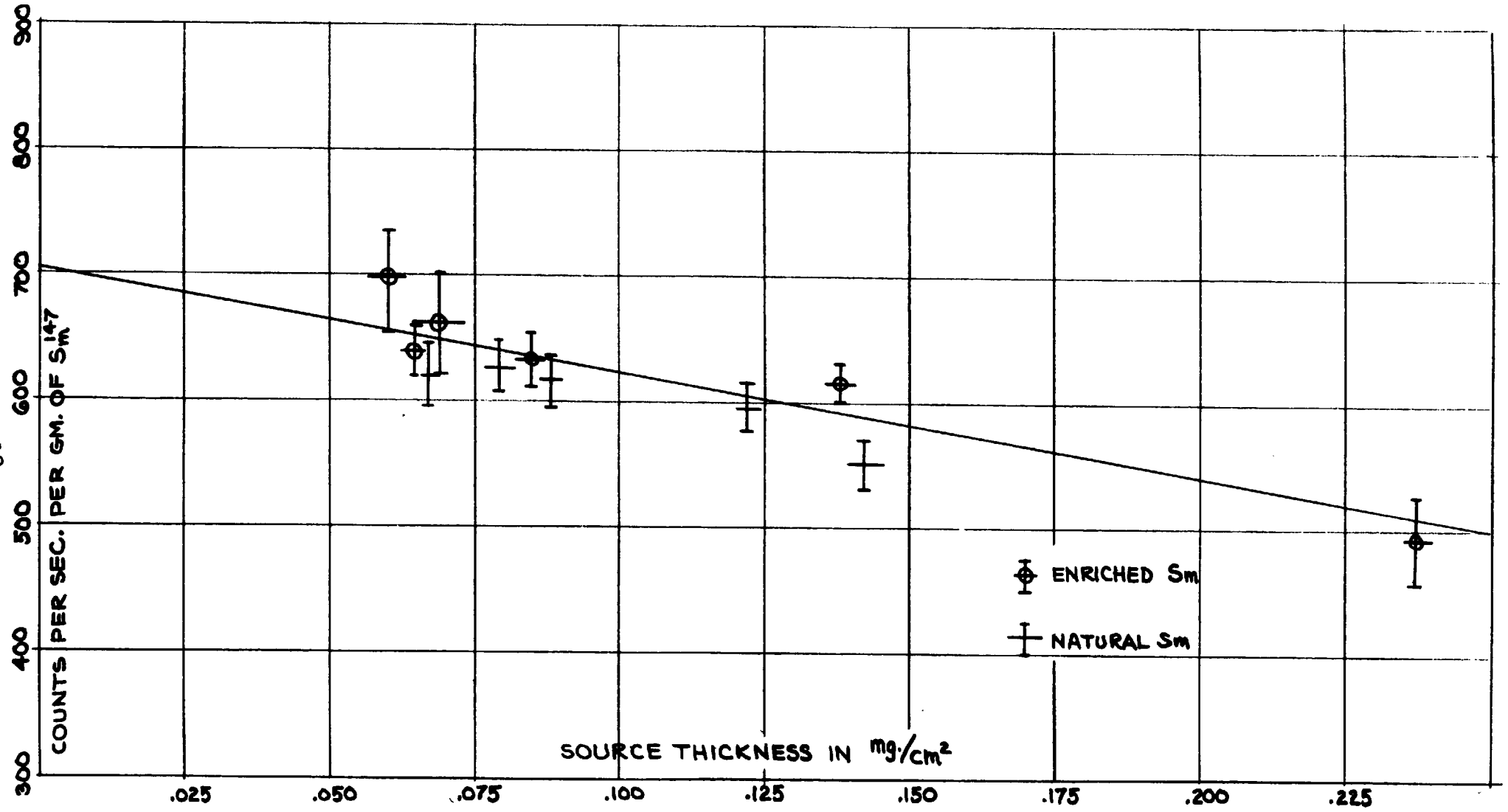


FIG. 4
HALF-LIFE EXTRAPOLATION

The best fit of a straight line[24] was made with the data, assuming equal errors for all points. While the data do not actually conform to this criterion the final result is surely well within the estimated possible error and agrees well with the results obtained if one makes a best fit drawn by eye. The intercept at zero source thickness gives a counting rate of 705 counts per sec per gm of Sm^{147}. After correcting for the counter inefficiency and including the experimental uncertainties one obtains a counting rate of 719 $\pm$ 36 counts/sec-gm Sm^{147}.

4. HALF-LIFE CALCULATION

The rate at which a radioactive isotope decays can be expressed as follows:

$$\frac{dn}{dt} = -\lambda n$$

where: n = the number of radioactive nuclei,

$\frac{dn}{dt}$ = number of disintegrations per second, and

λ = a constant characteristic of the particular isotope in question.

After integration one finds:

$$n = n_0 e^{-\lambda t} \qquad (1)$$

where: n_0 = number of nuclei present at $t = 0$.

The half-life, τ, is defined as the time necessary for $n = n_0/2$. Using this definition and Eq. (1) we find

$$\tau = \frac{\ln 2}{\lambda} = \frac{.693}{\lambda}$$

To find λ we take the experimentally obtained results for dn/dt. The half-life is then given by:

$$\tau = \frac{.693n}{dn/dt} \quad \frac{.693 \times 6.023 \times 10^{23}}{147 \times 719 \times 3.156 \times 10^{7}} = 1.25 \times 10^{11} \text{ years}$$

or, including the error:

$$\tau = 1.25 \pm .06 \times 10^{11} \text{ years}$$

5. ENERGY SPECTRUM

To investigate the energy spectrum 0.9 mg of enriched samarium chloride was evaporated onto a thin zapon film giving an average source thickness due to the samarium chloride of 0.008 mg/cm^2. The zapon film was then placed in contact with a fresh Eastman NTA 25 micron nuclear plate. After three weeks the plate and a blank control were examined using a microscope with the plate under oil immersion. Over 200 tracks were measured, but when a shrinkage factor of 2 was applied,[25,26] only 175 tracks were left which satisfied the criterion that their original penetration angles be less than 37.5°. Under these conditions an error of as much as 10% in the shrinkage factor would affect the length measurements by a maximum of about 4%. No alpha tracks were observed upon scanning a comparable area of the blank control plate.

Figure 5 shows the variation of the number of tracks per .3 micron intervals with the total range. From the distribution it appears that at least the large majority of the alpha particles are emitted at one energy. This is in agreement with the more recent results.[13,14,27-30] From the histogram one sees that the mean range is 7.0

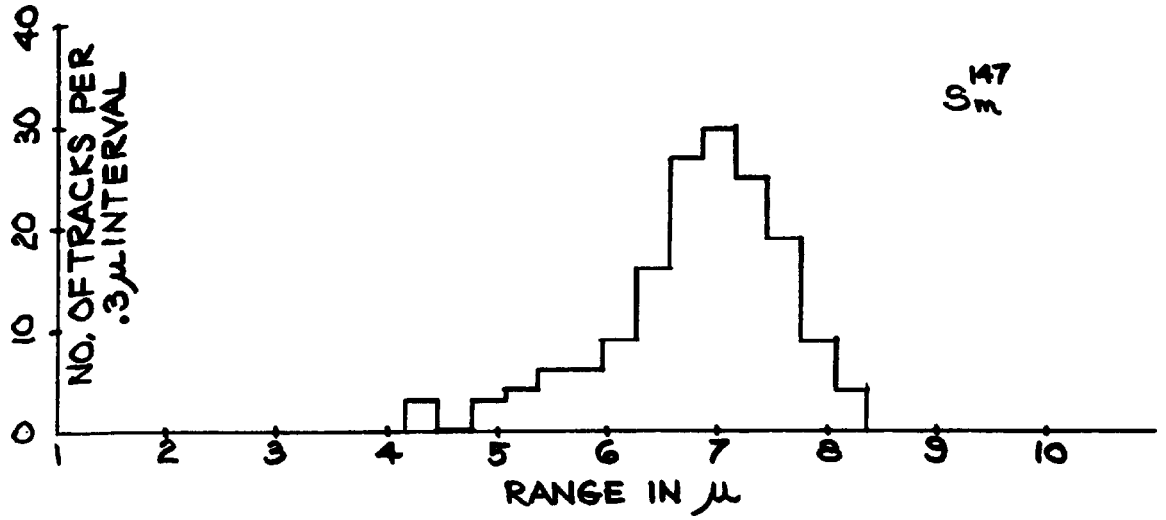


FIG. 5.
NUMBER OF TRACKS VS. RANGE FOR Sm^{147}

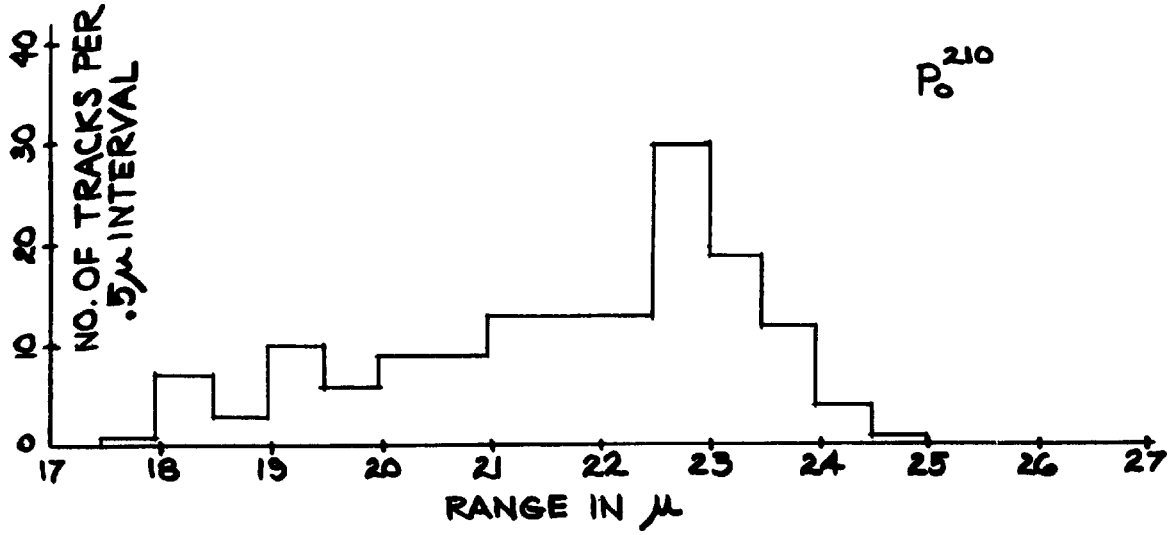


FIG. 6
NUMBER OF TRACKS VS. RANGE FOR Po^{210}

microns. It is rather difficult to assign an error to this type of measurement, but one can probably safely list the range as 7.0 ± .2 microns. If a range energy curve is drawn,[26] it can be seen that this corresponds to an energy of 2.11 ± .05 Mev.

Strictly speaking, this range-energy curve is based on data from Ilford B1 emulsions and while the range characteristics of these emulsions are very similar to the Kodak NTA emulsions they are not identical.[26] In an effort to calibrate the curve more closely, several drops of solution containing Po^{210} were allowed to dry on a zapon film and then placed in contact with another Eastman NTA 25 micron plate. The polonium alpha tracks were measured in the same way as was done with the Sm tracks and a histogram was made of the results. This is shown in Fig. 6.

The source was not microscopically uniform and a fair amount of self-absorption took place, as the relatively large number of shorter tracks indicates. But if one accepts these results then the peak indicates a range of 22.7 microns. From the range-energy curve this corresponds to an energy of 5.35 Mev. while other measurements using spectrometers[1] have given an energy of 5.30 Mev. so that there is fair agreement between the results of the two methods. This means that any adjustment one might wish to make in the range-energy curve to compensate for the difference in emulsions would undoubtedly have no significant effect in the value obtained for the energy.

An alpha energy of 2.11 ± .05 Mev. agrees well with a recent detailed emulsion measurement by Stzeinsznaider[30] who arrived at a value of 2.12 ± .03 Mev. This value is in disagreement with the results of Jesse and Sadauskis[31] who measured the ratio of the ionizations produced by samarium and polonium alphas in both argon and air.

They concluded that the relationship in air is not linear at low energies and so the energy of 2.07 Mev obtained for air is too low. However, they do assume a linear relationship in argon and quote a value of 2.18 $\pm$ .02 Mev for the alpha energy. Various authors[32-35] have questioned this assumption and there is now some doubt as to the validity of the result using argon.

Because the exact energy is of great significance in determining whether the theoretically predicted half-life agrees with the experimental value, it would be important to resolve the differences in the values of the energy as obtained by the different methods.

CHAPTER II

THEORY OF ALPHA DECAY

1. GENERAL DESCRIPTION

Alpha spectra may be either simple or complex. In the case of a simple spectrum only alpha particles of one well defined energy are emitted while in a complex spectrum alpha particles of two or more different energies may be found. The existence of complex spectra can be explained by assuming that the residual, or daughter muclei can be formed in any one of several quantized levels. The highest energy alpha particles are those emitted when the daughter nuclei are formed in the ground state and the lower energy alphas are those emitted when the daughters are left in the corresponding excited states. (See Fig. 7.) This assumption is very well corrobolated by measurements of the energies of the gamma rays emitted when the daughter nuclei decay from the excited states to their ground state.

There are, however, at least two cases known (ThC' and RaC') for which the above explanation does not hold. These nuclei emit a very few alpha particles with energies much larger than the main group and have lifetimes of less than a millisecond. The presence of the long range alphas in each case can be accounted for by the assumption that ThC' and RaC' nuclei are formed in excited states by beta decay and that occasionally before these excited states decay by gamma emission to the ground state they can decay directly by emission of

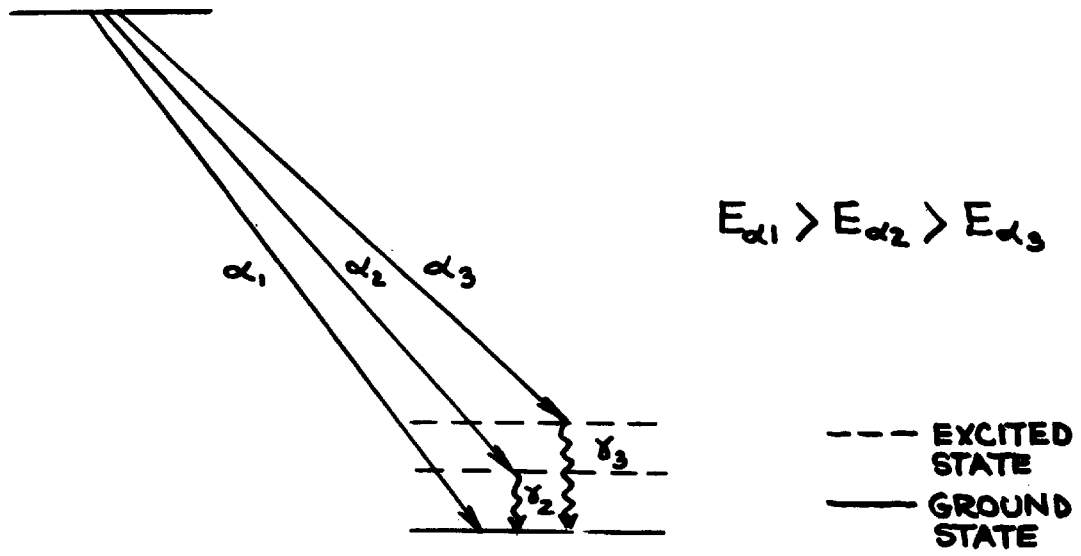


FIG. 7
COMPLEX ALPHA DECAY

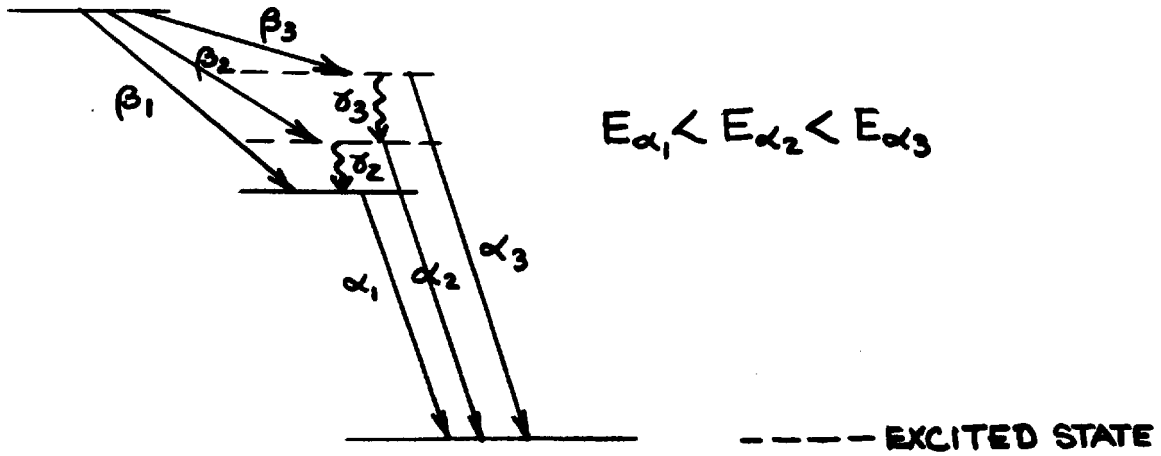


FIG. 8

COMPLEX ALPHA DECAY (Th C' & Ra C')

an alpha particle to the daughter nucleus. In these cases the particles will have an energy corresponding to the normal transition from the ground state of the parent to the daughter plus the energy of the corresponding excited state of the parent. (See Fig. 8.) Because the half-life for alpha decay is extremely energy dependent this extra energy makes it possible for the alpha emission to compete with the short lived gamma emission from the excited states.

2. ENERGY CONSIDERATIONS

If one considers the experimental results as well as semi-classical concepts the Weizsacker semi-empirical atomic mass formula can be set up. The formula can be written in the following form:[36]

$$n(A,Z) = 1.00813Z + 1.00898N - a_1A + a_2A^{2/3} + a_3\frac{(A/2-Z)}{A}$$

$$+ .000627\,\frac{Z^2}{A^{1/3}} + \delta\,(A,Z)$$

where: $1.00813Z$ and $1.00898N$ represent the masses of the constituent protons and neutrons when considered separately,

$-a_1A$ = volume energy correction; experimentally it is found that the binding energy is roughly proportional to the mass of the nucleus,

$a_2A^{2/3}$ = surface effect; analogous to the surface tension in a liquid,

$a_3\,\frac{(A/2-Z)}{A}$ = term due to the "symmetry energy"; correction for the number of unpaired nucleons,

$.000627\,\frac{Z^2}{A^{1/3}}$ = energy due to coulomb repulsion, and

$\delta\,(A,Z)$ = correction term depending upon stability of nuclei with respect to whether the number of Z and N is even or odd.

The values of the various constants, a_1, a_2, etc., are chosen to give results consistent with those obtained by experiment. These results are necessarily crude since many of the refinements in nuclear shell structure are not included. However, much useful information can be obtained. For instance, if we consider the binding energy of an alpha particle in a nucleus we find:

$$BE(\alpha) = M(A-4,Z-2) + 4.00390 - M(A,A)$$

The binding energy becomes negative in the middle of the periodic table indicating instability to alpha decay for the heavier elements. According to Kohman[37], who also considers some of the refinements to the theory, most nuclei with $A > 140$ are energetically capable of emitting alpha particles and are only stabilized by the nuclear potential barrier.

In the same way it can be seen that nuclei of even lower atomic number are unstable to fission. However, in this case the fission fragments have such large mass and charge that penetration of the potential barrier is much more difficult. Consequently, spontaneous fission is rare compared to alpha decay.

The fact that natural alpha decay is observed in the rare earth region for Sm^{147} and Nd^{144} is undoubtedly connected with the extra stability of the $n = 82$ configuration predicted by shell theory.[38] This extra stability affords an abnormally large amount of energy for the alpha particle thus permitting the decay to take place with observable life times. The work of Dunlavey and Seaborg[39] in detecting the alpha activity of artificially produced Sm^{146} is also in agreement with this idea.

3. THEORETICAL TREATMENT

Modern theoretical treatments of alpha decay stem directly from the work of Gamow[40] and Gurney and Condon[41] who first introduced the concept of quantum mechanical penetration of the coulomb barrier to explain the relationship between half-life and energy in alpha emission.

a. One Body Model

The original theory is based on the one body model with the alpha particle being assumed to exist in the nucleus and to move in a potential created by the nucleus. Inside the nucleus the potential is assumed to have some constant value V_0. (V_0 is not well defined, but its exact value is not very important and in any case it is less than the energy which the alpha particle must have in order to penetrate the coulomb barrier.) Outside the nucleus, beyond the range of the nuclear forces, there is only the regular coulomb potential between the daughter nucleus and the alpha particle. This potential is given by:

$$V_c = \frac{zZe^2}{r}$$

where: ze = charge of the alpha particle,
Ze = charge of the residual nucleus,
r = distance between centers of the alpha particle and residual nucleus.

The potential reaches a maximum at $r = R$.

$$V_{c_{max}} = \frac{zZe^2}{R}$$

where: R = the sum of the nuclear radius and the effective radius of the alpha particle.

Figure 9 shows a plot of the potential with the further assumption that the alpha particle is emitted in an s ($\ell=0$) state. For a particle of energy E it can be divided into three regions.

1) inside the nucleus where $r<R$ and $E>V(r) = V_0$

2) the potential barrier region where $R<r<\frac{zZe^2}{E}$ and $V(r)>E$

3) outside the nucleus where $r>\frac{zZe^2}{E}$ and $E>V(r)$

Classically, an alpha particle of energy E, which is less than the maximum of the coulomb barrier, would not be able to escape. Everytime it came up against the barrier it would merely reverse directions. However, according to quantum mechanics there is a finite chance for the particle to penetrate the barrier and thus escape.

If we consider an alpha particle moving in the nucleus its wave function ψ satisfies the wave equation:

$$\nabla^2\psi + \frac{2M}{\hbar^2}(E-V(r))\psi = 0 \qquad (2)$$

M = reduced mass of the alpha particle.

E = energy of the alpha particle inside the nucleus (= available nuclear decay energy).

V(r) = spherically symmetric potential.

The number of particles which leave the nucleus per unit time is then:

$$N = 4\pi r^2 v \, |\psi|^2$$

where v is the velocity of the α particle in the nucleus.

In general the wave function can be expanded in a series of subwaves of orbital angular momentum .

$$\psi(\vec{r}) = \psi(r,\theta) = \sum_{\ell=0}^{\infty} \frac{U_\ell(r)}{r} Y_{\ell,0}(\theta) \qquad (3)$$

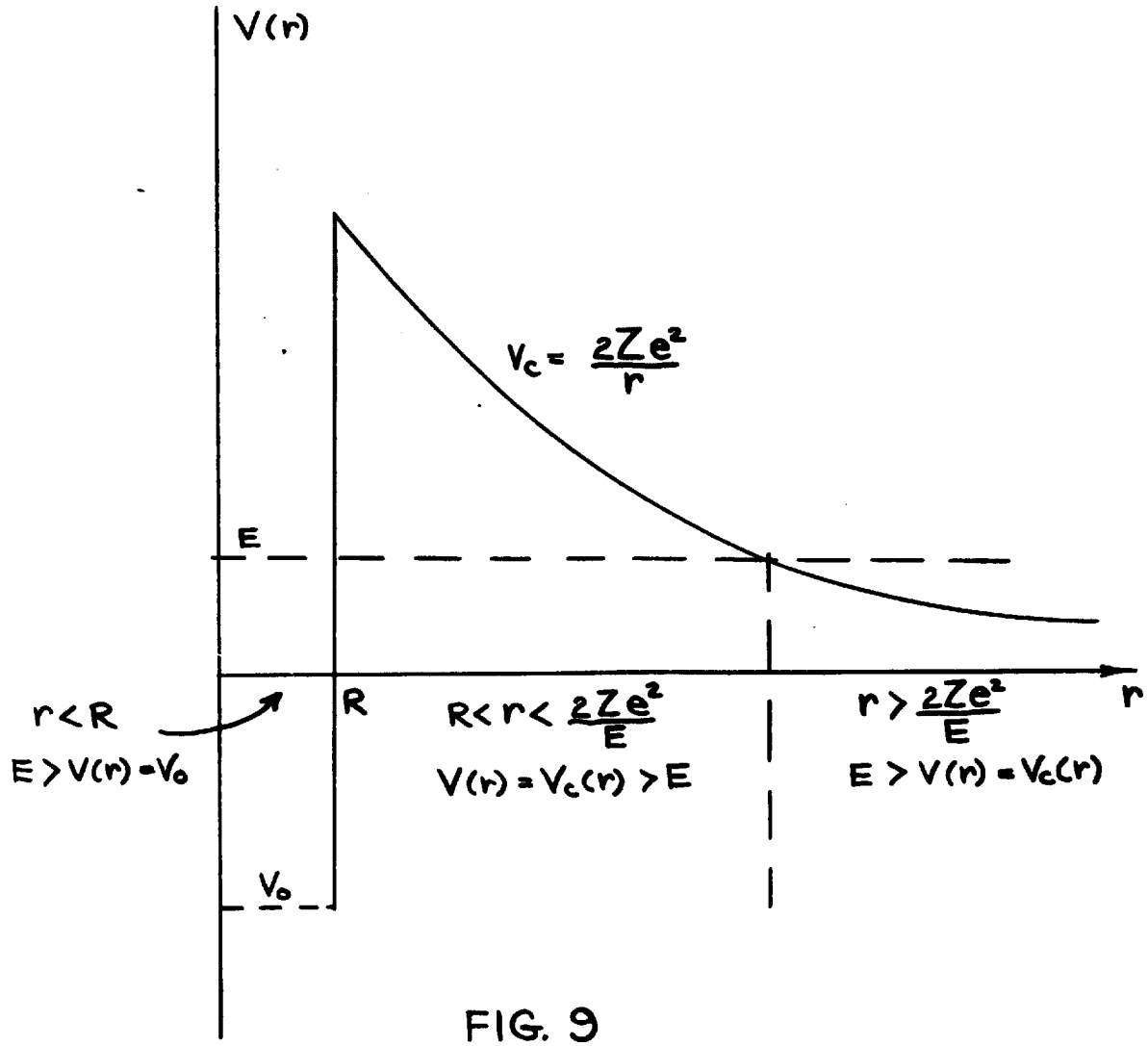


FIG. 9

V(r) FOR ALPHA PARTICLE EMITTED IN S STATE

$Y_{\ell,0}(\theta)$ are spherical harmonics.[42]

If we now assume that the alpha particle is moving in an s state then

$$\psi = \frac{U_0}{r} = \frac{U}{r} \qquad (\ell = 0)$$

and the wave equation becomes:

$$\frac{d^2U}{dr^2} + \frac{2M}{\hbar^2}(E-V)U = 0 \tag{4}$$

This equation is best solved using the WKB approximation. When this is done[44] one obtains an expression for the activity of the form:

$$\lambda = fP = \text{number of alpha particles emitted per second} \tag{5}$$

P is the famous penetrability factor.

$$P = e^{-2c} = e^{-\frac{2}{\hbar}\sqrt{2M}\int_R^{Y_E}(zZe^2r^{-1}-E)^{1/2}dr}$$

A straightforward integration gives:

$$c = \frac{\sqrt{2M}}{\hbar}\frac{zZe^2}{E^{1/2}}\left[\cos^{-1}\left(\frac{ER}{zZe^2}\right)^{1/2} - \left(\frac{ER}{zZe^2}\right)^{1/2}\left(1-\frac{ER}{zZe^2}\right)^{1/2}\right]$$

or

$$c = \frac{2zZe^2}{\hbar v}\left[\cos^{-1}X^{1/2} - X^{1/2}(1-X)^{1/2}\right] \quad \text{where } X = \frac{ER}{zZe^2}$$

The quantity f corresponds roughly to the frequency of the periodic motion expected of any particle in a bound state.

b. Many Body Model

The one body theory of alpha decay is open to criticism on the grounds that it assumes that the alpha particle exists as a unit

moving freely inside the nucleus in a potential created by the residual nucleus. Instead, one could just as well assume that in general the components of the alpha particle would not be distinguishable from the other nuclear particles, but that they join together to become an alpha particle just at the moment of emission. For a simplified discussion one can say that the probability for alpha decay would be the product of two factors:

1) The probability of finding the nucleus in a configuration such that an alpha particle appears at the potential barrier.
2) The probability that the alpha particle will penetrate the barrier and escape.

Following Blatt and Weiskopf[43] we can write:

$$\lambda = \omega_0 T$$

ω_0 = the number of attempts per second to penetrate the potential barrier,

T = transmission coefficient of the barrier.

Now we know that the motion in a bound state has a periodic character so it seems reasonable to identify ω_0 with the classical period $\overline{P}$. Then, going further, one can use a rough approximation between the classical period and the level distance, D , between levels of the same parity and angular momentum.

$$\omega_0 = \overline{P}^{-1} \sim \frac{D}{2\pi\hbar}$$

Then

$$\lambda \approx \frac{D}{2\pi\hbar} T$$

This result is the same as that obtained by a more rigorous quantum mechanical treatment.[43] The calculation of the transmission

coefficient is usually carried out by means of the WKB approximation and one obtains the factor P, so that again the activity can be expressed in the form of Eq. (4), but here the f may have a very different value than the one obtained using the one body approach. For instance, in the extremes of the one body and many body models described by Bethe[44], the values of f differ by a factor of 10^6.

c. Penetration Factor

It is the exponential nature of P that makes the decay rate for both models so sensitive to changes in the nuclear variables as exemplified by the fact that a change in the alpha particle energy by a factor of about 2 can change the half-life by a factor of 10^{24}. The exponential is also very sensitive to the value of R. A variation in R of about 17% changes the theoretical value by a factor of 100 for E = 2.2 Mev. Therefore, even though f is not well known, the experimentally measured values of λ and E can be used to determine the value of R with fair accuracy.

From the calculated value of R one would like to obtain the corresponding value of the radius of the residual nucleus. However, here again there is some uncertainty. R is really a sort of effective distance between the centers of the residual nucleus and alpha particle since one would expect some coulomb repulsion effects to be felt even before the alpha particle had fully left the nucleus. Accordingly, R would not be equal to the sum of the radii of the alpha particle and daughter nucleus but would equal a somewhat smaller value. This means that in any given case we must set

$$R = R_X + \rho_\alpha$$

where: R_X = the nuclear radius of the daughter nucleus,

ρ_α = the effective radius of the alpha particle and is smaller than the actual radius as determined by other means.

If a reasonable value for ρ_α is assumed, consistent results for the various nuclear radii can be obtained. These radii will differ, however, depending on what model is used to determine f. If one considers the extremes previously mentioned, when the experimental measurements of decay rate and alpha energy are used to determine the nuclear radius the value obtained using the many body model is always about 40% greater than that obtained using the one body model.

d. Angular Momentum of the Alpha Particle

So far no mention has been made of the possibility of a change in the nuclear spin during the disintegration although such a change does sometimes occur. Since the spin of the alpha particle is zero any nuclear spin change must result in a non-zero angular momentum of the alpha particle. To see the effect of this we can substitute Eq. (3) into the wave equation, Eq. (2) and find:

$$\frac{d^2U_\ell}{dr^2} + \frac{2M}{\hbar^2}\left[E - \frac{\ell(\ell+1)\hbar^2}{2r^2M} - V(r)\right] U_\ell = 0 \qquad (6)$$

Comparing Eqs. (4) and (6) we see that the inclusion of alpha particles with angular momentum is equivalent to adding another term to the potential barrier height, which taken by itself means that the higher the value of ℓ the lower the probability for decay will be. The maximum of the potential barrier becomes:

$$\frac{zZe^2}{R} + \frac{\ell(\ell+1)\hbar^2}{2M_\alpha R^2}$$

$\ell\hbar$ = angular momentum carried away by the alpha particle

The ratio of the angular momentum term at the maximum to the coulomb term is:

$$\ell(\ell+1)\,\frac{1.80}{ZR}$$

where R is in terms of 10^{-13}cm. When $r > R$ this ratio becomes even smaller.

For the usual values of R and Z this term does not give any appreciable contribution for low values of ℓ in comparison to the uncertainty already existing in the choice of values for f. Of course one must take into account the conservation laws of angular momentum and parity when considering possible values for the ℓ of the emitted alpha particle.

CHAPTER III

COMPARISON OF THE EXPERIMENTAL RESULTS WITH THE THEORY

Rasmussen, Thompson, and Ghiorso[45] have calculated the decay constant of various rare earth isotopes using five different decay formulas. These formulas all have the form $\lambda = fP$, but they differ in the formulation of f. The values used for R were based on the experimental decay rate of Gd^{148}. This isotope has an even-even nucleus and presumably should undergo a parity-favored decay with the alpha particle being emitted in an s state, whereas a nucleus with an odd number of nucleons could have its decay hindered by various factors such as a change in spin. In the calculations the reduced mass and total nuclear decay energies were used. The total nuclear decay energy can be obtained from the measured kinetic energy of the alpha particle by adding the calculated nuclear recoil energy as well as a correction term equal to the electrostatic potential energy of the alpha particle at the nucleus due to the electron cloud.[45]

For Sm^{147}, considering the alpha energy to be 2.18 Mev, they obtained a half-life of 1.6×10^{12} years when using the formula by Rasmussen. This is more than 10 times as long as the experimental value of 1.25×10^{11} years.

The decay rate is so dependent on the value of the decay energy that a difference of around 70 kev corresponds to a change in the decay rate by a factor of ten. Consequently, a 3% increase in the

measured alpha energy would give approximate agreement between the measured and predicted half-lifes. However, as was noted previously, the latest energy measurement using nuclear emulsions gives an energy of 2.12 mev which is 3% lower, and would predict a half-life about 100 times as great as that observed. This difference is of all the more interest as it results from an observed activity which is greater than the predicted value and thus cannot be explained by assuming that the transition is hindered in some way because we are dealing with an odd nucleon nucleus.

Since the discrepancy between the calculated and measured activities is so large and contradictory to the theoretical predictions it seems worthwhile to speculate about the situation to see whether the difference perhaps has some fundamental significance or if it can be explained by fairly elementary considerations.

Figure 10 shows a plot of log $(1/\lambda)$ against the total decay energy and Fig. 11 gives the variation of log $(1/\lambda)$ with the effective nuclear radius, where λ = the decay activity per second. The formula employed for the calculations was one used by Biwas and Patro[46] and by Perlman and Ypsilantis[47].

$$\lambda = \frac{v}{R} P$$

with v = the velocity of the alpha particle in the center of mass system and R = the effective nuclear radius and was taken to be = 7.55×10^{-13} cm from the empirical results of Rasmussen et al[45] for Gd^{148}. P is the penetration factor already introduced.

As can be seen from the figures in order to get agreement between the experimental and the theoretical values of log $(1/\lambda)$ one

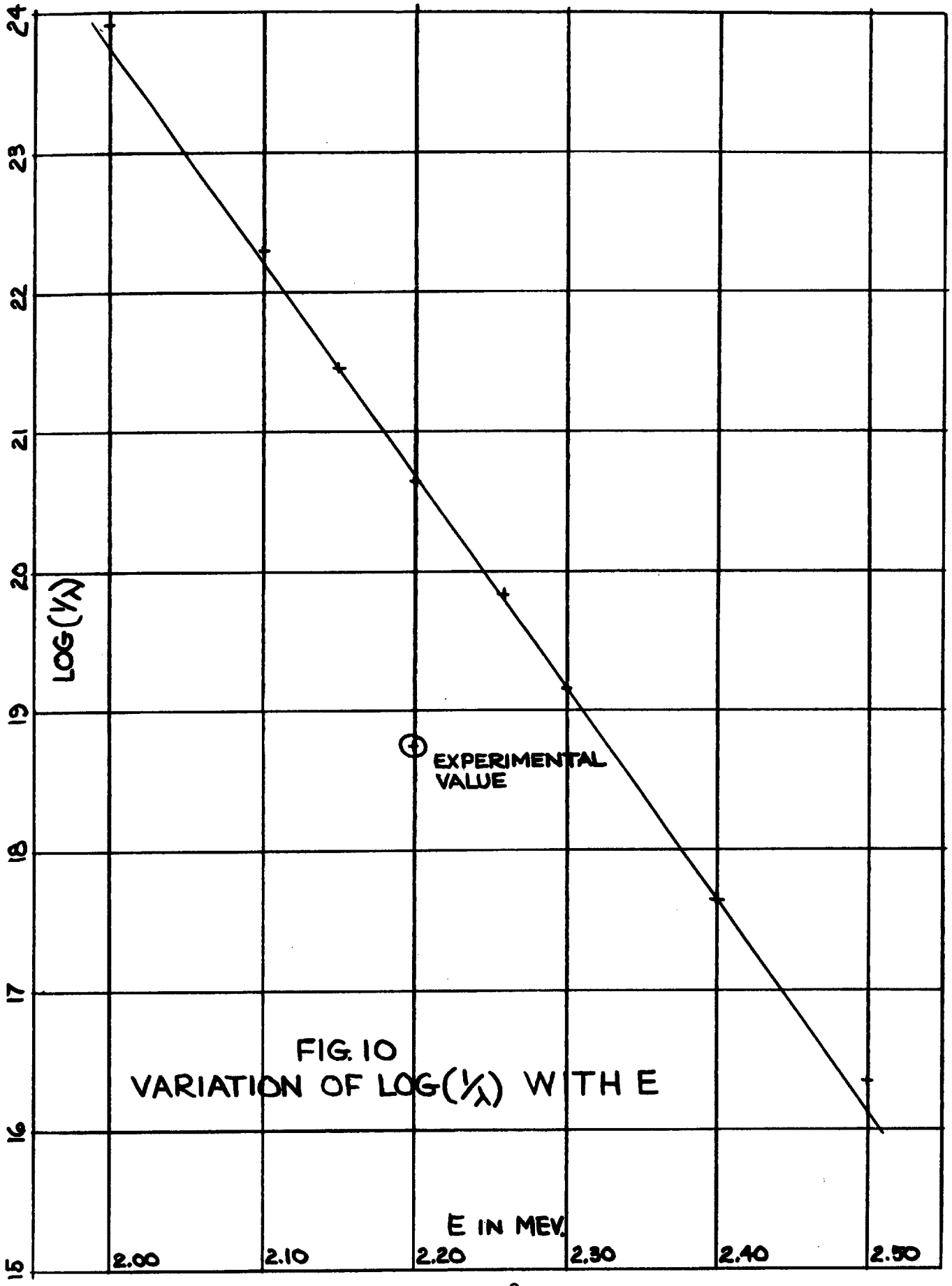


FIG. 10
VARIATION OF LOG(1/λ) WITH E

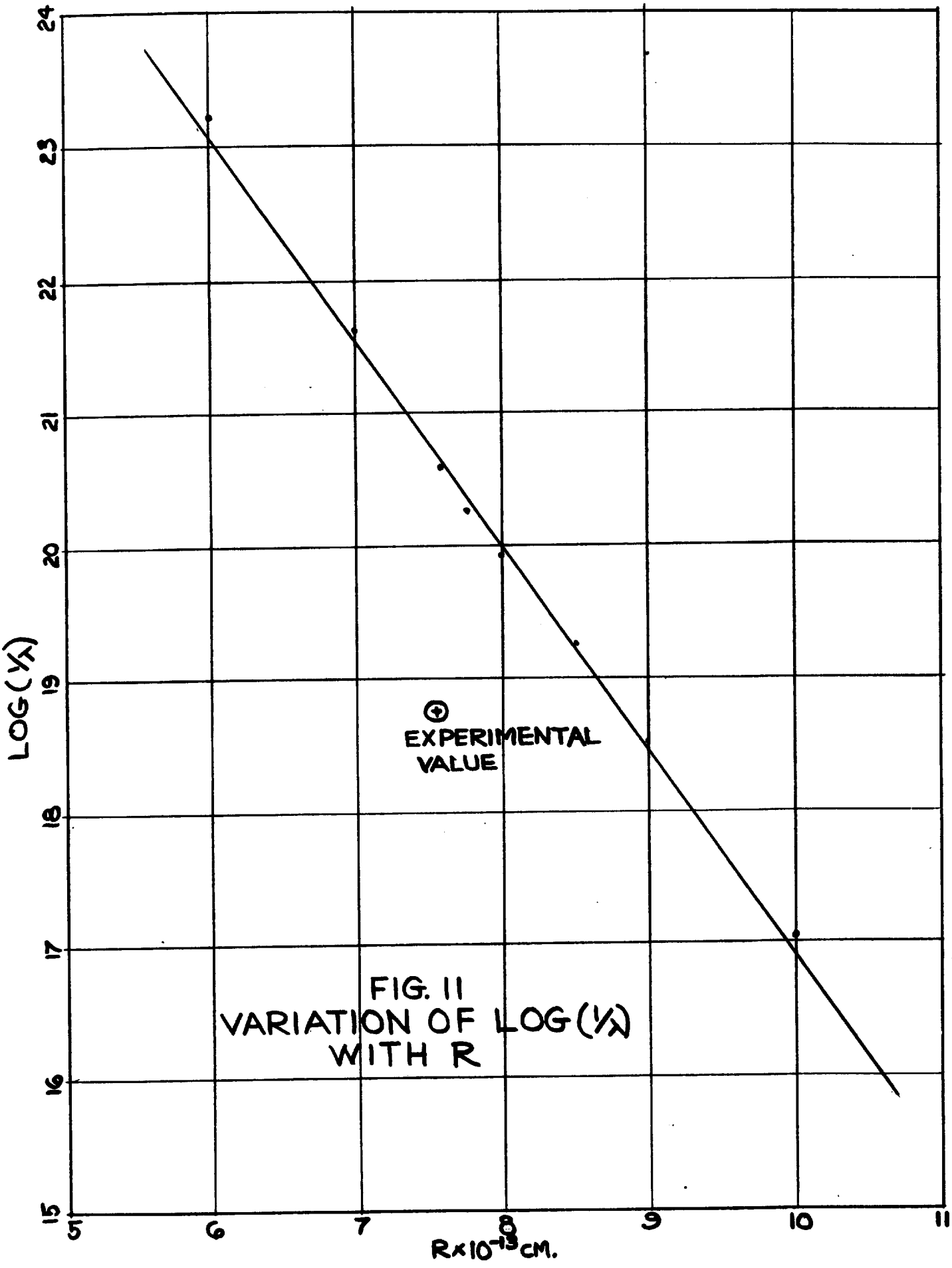


FIG. 11
VARIATION OF LOG(1/λ)
WITH R

would need either to assume an increase in the radius by 17% or the energy by 6.4%. While there is still some uncertainty in the exact value of the alpha decay energy as well as an estimated possible 5% error in the nuclear radius, it appears quite unlikely that these errors could account for all of the discrepancy between the decay rates.

Assuming the difference in the decay rates to be real, perhaps some unusual aspect of the nuclei involved might help give an explanation. According to the table of nuclear moments in Ramsey[48] the spin of the Sm^{147} nucleus is 5/2 while that of Nd^{143}, the daughter nucleus, is given as 7/2. However, later work by Bogle and Scovil[49] shows that the spin of Sm^{147} is really 7/2 also so that there is no spin change in the alpha decay of Sm^{147} which helps make the transition more favored.

It was also noted that in this region various nuclei have abnormally large and positive quadrupole moments. Although the quadrupole moments for Sm and Nd are not known it seems reasonable to suppose that the value for Nd^{143} might also be large and positive. In such an event the charge distribution could be taken to be uniform and to form an ellipsoid of revolution with the major axis along the direction of spin. Then the coulomb barrier that the alpha particle must penetrate might be distorted in such a way as to allow the alpha particle to escape more readily than from a purely spherical charge distribution. Or one could still assume a spherical nucleus and calculate the effect of adding the quadrupole field to the usual monopole component. To make the conclusions more quantitative an approximate calculation was made.

In general, assuming the alpha particle carries away zero angular momentum, we have from previous considerations that

$$P = e^{-2c}$$

where

$$c = \frac{(2M)^{1/2}}{\hbar} \int_R^{Y_E} \left\{ V(r,\theta) - E \right\}^{1/2} dr$$

and

$$V(r,\theta) = \frac{1}{r} \sum_{n=0}^{\infty} \frac{A_n}{r^n} P_n(\cos\theta) = \frac{zZe^2}{r} + \phi_2(r,\theta)$$

$\phi_2(r,\theta)$ = quadrupole potential with θ being the angle with respect to the z axis (which points along the spin axis).

$$\phi_2(r,\theta) = \frac{1}{2} \frac{A_2}{r^3} (3\cos^2\theta - 1)$$

and for an ellipsoidal charge distribution

$$A_2 = \frac{1}{2} \int \rho(r')(3z'^2 - r'^2) d\tau'$$

By definition

$$Q = \frac{2}{e} A_2 = \text{quadrupole moment}$$

so

$$\phi_2(r,\theta) = \frac{Qe}{4r^2} (3\cos^2\theta - 1) \text{ per unit charge}$$

or for an alpha particle of charge ze

$$\phi_2(r,\theta) = \frac{Qe^2 z}{4r^2} (3\cos^2\theta - 1)$$

Then

$$c = \frac{(2M)^{1/2}}{\hbar} \int_R^{Y_E} \left\{ \frac{zZe^2}{r} + \frac{Qe^2 z}{4r^3} (3\cos^2\theta - 1) - E \right\}^{1/2} dr$$

$$c = \frac{(2MzZe^2)^{1/2}}{\hbar} \left\{ \int_R^{P} \frac{1}{\sqrt{r}} \left[1 + \frac{Q(3\cos^2\theta - 1)}{4r^2 Z} - \frac{Er}{zZe^2} \right]^{1/2} dr \right.$$

$$\left. + \int_P^{Y_E} \left[1 - \frac{Er}{zZe^2} \right]^{1/2} dr \right\}$$

where ρ is the value of r beyond which the quadrupole term ceases to make an effective contribution. For any given value of Q it can readily be determined graphically. In the first integral where

$\rho > r > R$

$$\frac{Q(3\cos\theta-1)}{4r^2Z} < 1 \qquad \text{and} \qquad \frac{Er}{zZe^2} < 1$$

one can expand the square root and get, keeping only significant terms,

$$A = \int_R^{\rho} \frac{1}{\sqrt{r}}\left\{1 + \frac{Q(3\cos^2\theta-1)}{8r^2Z} - \frac{Er}{2zZe^2} - \frac{1}{8}\frac{E^2r^2}{zZe^2}\right\} dr$$

$$= X\left\{2(\sqrt{X\rho} - \sqrt{XR}) - \frac{1}{8}\frac{QX^2(3\cos\theta-1)}{12Z}\left[\frac{1}{(X\rho)^{3/2}} - \frac{1}{(XR)^{3/2}}\right]\right.$$

$$\left. - \frac{1}{3}((X\rho)^{3/2} - (XR)^{3/2}) - \frac{1}{20}((X\rho)^{5/2} - (XR)^{5/2})\right\}$$

where $X = \sqrt{\frac{E}{zZe^2}}$

If one chooses $Q = 6 \times 10^{-24}\,cm^2$, $\rho = 35 \times 10^{-13}$ cm for the case when $E = 2.20$ Mev, $z = 2$, $Z = 60$ and $R = 7.55 \times 10^{-13}$cm

$$A = \frac{(2M)^{1/2}}{\hbar}\frac{zZe^2}{\sqrt{E}}\left\{.617 + .004(3\cos^2\theta-1)\right\}$$

An exact integration for A without the quadrupole term gives

$$A = \frac{(2M)^{1/2}}{\hbar}\frac{zZe^2}{\sqrt{E}}\left\{(X\rho)^{1/2}(1-X\rho)^{1/2} - (XR)^{1/2}(1-XR)^{1/2} + \sin^{-1}(X\rho)^{1/2} - \sin^{-1}(XR)^{1/2}\right\}$$

$$= \frac{(2M)^{1/2}}{\hbar}\frac{zZe^2}{\sqrt{E}}\,(.618)$$

The agreement is within the sliderule accuracy used and justifies the approximation in the expansion.

Since the total value for C using the exact expression is

$$C = \frac{(2M)^{1/2}}{\hbar} \frac{zZe^2}{\sqrt{E}} \quad (.915)$$

we see that even under the most favorable conditions with $\theta = \frac{\pi}{2}$ the quadrupole potential can have little effect on the activity if we assume a spherical nucleus. However, if instead of a spherical nucleus one assumes that the nucleus is elliptical in shape, then at the ends along the z axis R increases and so the overall coulomb barrier height might be expected to decrease.

For a uniform elliptical charge distribution a simple calculation gives an approximate relationship between the ratio of the axis and the quadrupole moment

$$d \approx \frac{5Q}{4ZR^2} = .22$$

where d is defined by the relation $a = b(1+d)$, a = major axis and b = minor axis.

This compares with the 17% increase in the nuclear radius needed to give agreement between the observed and calculated decay rates for a spherical nucleus. To see the effect on P we can take $d = .20$ and then $R = 9.06 \times 10^{-13}$ cm

$$A = \frac{(2M)^{1/2}}{\hbar} \frac{zZe^2}{\sqrt{E}} \quad (.565 + .003(3\cos^2\theta - 1)) = \frac{(2M)^{1/2}}{\hbar} \frac{zZe^2}{\sqrt{E}} \quad (.571)$$

for $\theta = 0$.

The change in C = 5.03% and the activity increases by a factor of

$$e^{96.2 \times .0503} = 125$$

This, of course, has only the roughest sort of calculation and ignores among other things the fact that the theory was developed for a spherical nucleus with a spherically symmetric potential giving a 4π geometry for emission. However, it does give an indication that perhaps some sort of abnormal nuclear deformation, under which the nuclear potential well is no longer completely spherically symmetric, could explain the discrepancy between the two activities without the necessity of a fundamental change in the present theory of alpha decay. Until more information becomes available on the Sm and Nd nuclei this is about all that one can say.

CHAPTER IV

BETA ACTIVITY OF K^{40} AND K^{42}

1. HISTORY OF BETA SPECTRUM MEASUREMENTS OF K^{40}

The beta decay of K^{40} takes place with a spin change of 4.[50] From this and other theoretical considerations Marshak[51] and Greuling[52] have predicted that the beta spectrum should be of the unique third-forbidden type. Several attempts have been made in recent years to observe the spectrum to see if it agrees with the theoretical prediction.

Using a lens spectrometer Alburger[53] at first found the Fermi plot of the K^{40} beta spectrum to have an allowed shape above 500 kev, but subsequent events showed that this result was undoubtedly due to distortion introduced by the use of a non-uniform thick source. At a later time Alburger[54] reported an unallowed Fermi plot that could be made linear above 500 kev by applying the appropriate correction factor. However, he also found that the unique second-forbidden correction factor could be used to make the Fermi plot linear in the same region. Since these factors are very similar it is necessary to obtain the beta spectrum in great detail, especially at low energies, in order to distinguish between them.

Feldman and Wu[55] also used a beta spectrometer (solonoid type) to measure the spectrum and obtained results in agreement with those of Alburger. The corrected Fermi plot was linear above 500 kev and they concluded that the deviation which occurred for lower energies was very likely due to the source thickness.

The problem was attacked somewhat differently by Bell, Weaver and Cassidy[56] who employed a scintillation spectrometer. The source consisted of KCl mounted on polyethylene with an anthracene crystal used as the scintillation phosphor. Their measurement gave a non-linear Fermi plot that could be linearized above 700 kev.

Even though potassium sources of enriched K^{40} abundance were available the problem of obtaining a sufficient activity necessitated the use of relatively thick sources for all these investigations. Consequently, large amounts of distortion were introduced into the spectrum and the non-linearity of the corrected Fermi plots at lower energies was not surprising.

To circumvent this difficulty Good[57] obtained a thallium activated KI crystal to act as the scintillation element of a scintillation spectrometer. By measuring the activity of the K^{40} in the crystal itself he was able to obtain a comparitively large activity with an effective zero source thickness. However, he also was compelled to make fairly large corrections to his data. Because a small crystal weighing only 5.26 grams was used, a relatively large number of electrons were able to reach the surface before expending all their energy in the crystal. Although Good mentions no figures, an approximate calculation shows that about 16% of the 1.2 mev electrons did not lose all their energy within the crystal and gives an idea of the magnitude of the overall correction.

Besides this a correction had to be made for the finite resolution of the spectrometer as well as the fact that the KI crystal absorbs some of its own gamma radiation. This latter correction is quite small, but the resolution correction is by no means negligible

especially at the high energy end of the spectrum. Finally, at the low energy end of the spectrum he had to consider the background count due predominantly to photomultiplier noise. The background becomes so great that the spectrum cannot be measured below 100 kev.

In spite of these difficulties Good obtained a corrected Fermi plot approximately linear down to 300 kev which was a distinct improvement over previous results.

More recently Marshall(58) has measured the spectrum using a liquid argon ionization chamber. A very large amount of distortion was introduced into the spectrum by the large backscattering of the beta particles in the chamber. This was corrected for by observing the distortions of the spectra of Y^{91} and P^{32} due to backscattering and noting the correction factors necessary to bring the distorted spectra back to their known shapes. The Fermi plot was then linear above 500 kev when the unique third-forbidden correction factor was applied.

Since an appreciably larger KI crystal than that used by Good was available it was decided to reinvestigate the K^{40} beta spectrum using a scintillation spectrometer. With the larger KI crystal the surface correction term becomes smaller and there is an increase in the measured activity which facilitates the collection of data. Using this crystal with an improved spectrometer giving better resolution it was hoped that the spectrum could be measured in sufficient detail to distinguish between the various correction factors.

2. SCINTILLATION SPECTROMETER

The scintillation spectrometer was of conventional design. The scintillation element consisted of the thallium activated KI crystal. It weighed 30.96 grams and was cylindrical in shape. Good optical contact with the Dumont 6292 photomultiplier tube was maintained by using a thin layer of Dow Corning grease between one end of the crystal and the cathode surface. Magnesium oxide powder was packed around the crystal to minimize the light loss through the walls and thereby improve the overall resolution. A simple high voltage supply regulated by a string of ODC VR tubes furnished the operating potential. The output of the photomultiplier was fed through a cathode follower into a Model 204B Atomic Instrument Linear Amplifier. From the amplifier the pulses went to a pulse analyzer. The pulse analyzer consisted of a single channel discriminator based on a design by Johnstone[59] and modified by Lu.[60] When first tested it was discovered that the discriminator did not respond well to the comparitively slow rising pulses ($\sim .6\,\mu s$) from the amplifier, but after a minor change in the circuit the trouble disappeared. The discriminator output pulses were fed into a Nuclear Instrument Model 161 scalar with Mercury register.

To compare the performance of the spectrometer with that of similar types, a NaI crystal (3/4" by 1" dia.) was substituted for the KI crystal and the gamma ray spectrum of Co^{60} was observed. Figure 12 shows the result. The resolution of the 1.33 mev peak was 7-1/2%.

Using the KI crystal the linearity and resolution were checked at 5 different energies with gamma rays from

Zn^{65} (1.12 Mev)
Cs^{137} (.661 Mev)
Au^{198} (.411 Mev)
I^{131} (.364 Mev)
Ce^{144} (.134 Mev)

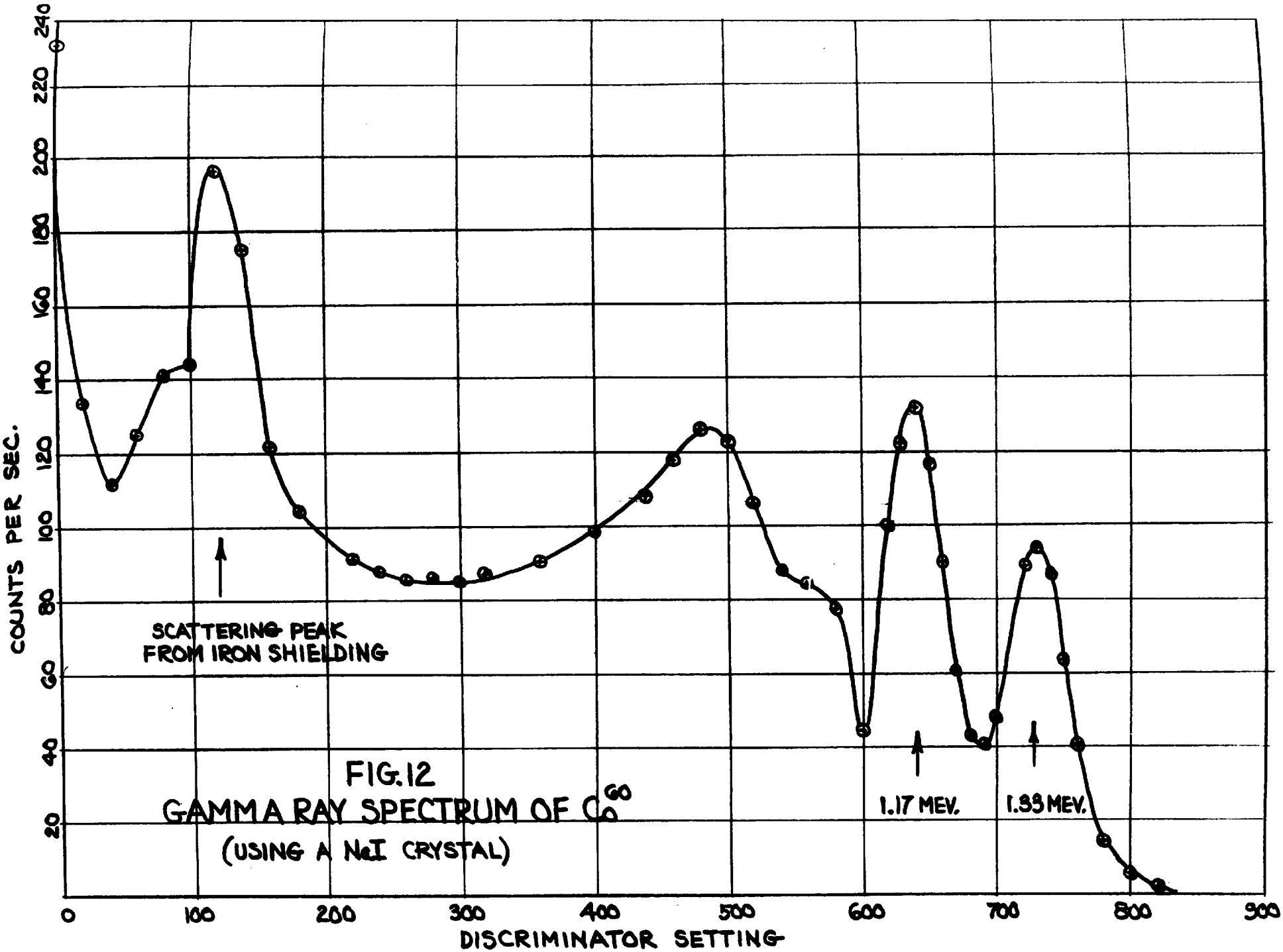


FIG. 12

GAMMA RAY SPECTRUM OF Co^{60}

(USING A NaI CRYSTAL)

The gain of the amplifier was then decreased by a factor of two and the points corresponding to the Ce^{144}, I^{131} and Cs^{137} gamma ray energies were noted. The values were plotted against the discriminator pulse height setting and, as Fig. 13 shows, they fell along a straight line thereby demonstrating that the spectrometer had good linearity.

3. K^{40} BETA SPECTRUM

While measuring the beta spectrum the energy calibration was checked at intervals using the Zn^{65} gamma ray at 1.12 mev and the discriminator pulse height reading for this peak was maintained to within one per cent. A 25 kev channel width was used and sufficient data recorded such that the low energy points had standard deviations of around 1%. In the upper end of the spectrum the statistical uncertainties became somewhat greater and the standard deviations were about 1.5%. To investigate the low energy end of the spectrum in more detail the amplifier gain was increased by a factor of two using the Cs^{137} peak for calibration. Then to insure that no spurious counts were being recorded because of delayed multiple counts at low energies, various dead times were introduced into the recording circuit using a univibrator arrangement with a variable output pulse length. Figure 14 shows the close agreement between the low energy points of the spectrum measured at twice normal amplifier gain with a normal apparatus dead time of several microseconds and those points recorded using a dead time of 4000 μs and the same amplifier gain. Intermediate dead time values gave similar results.

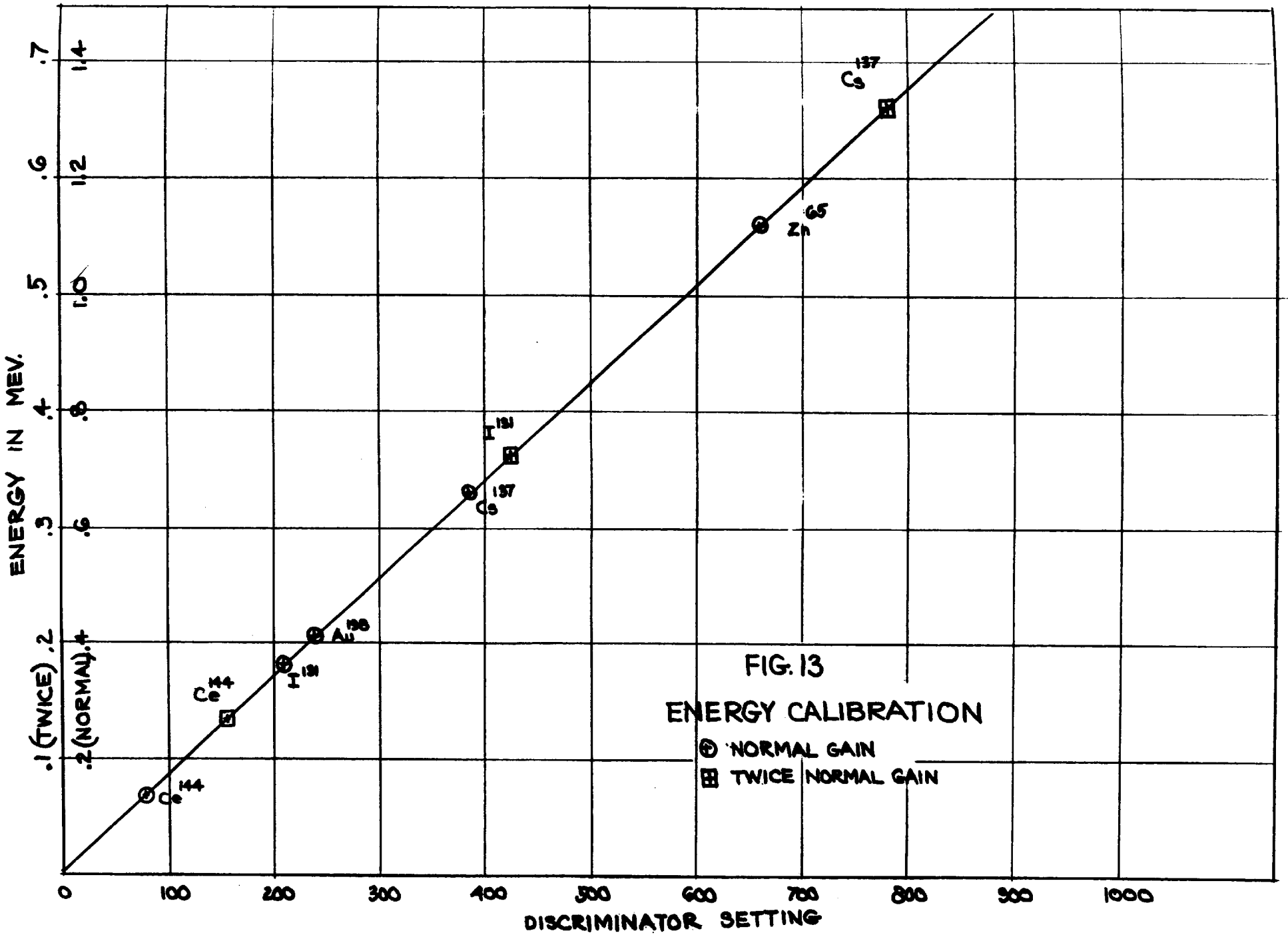


FIG. 13

ENERGY CALIBRATION

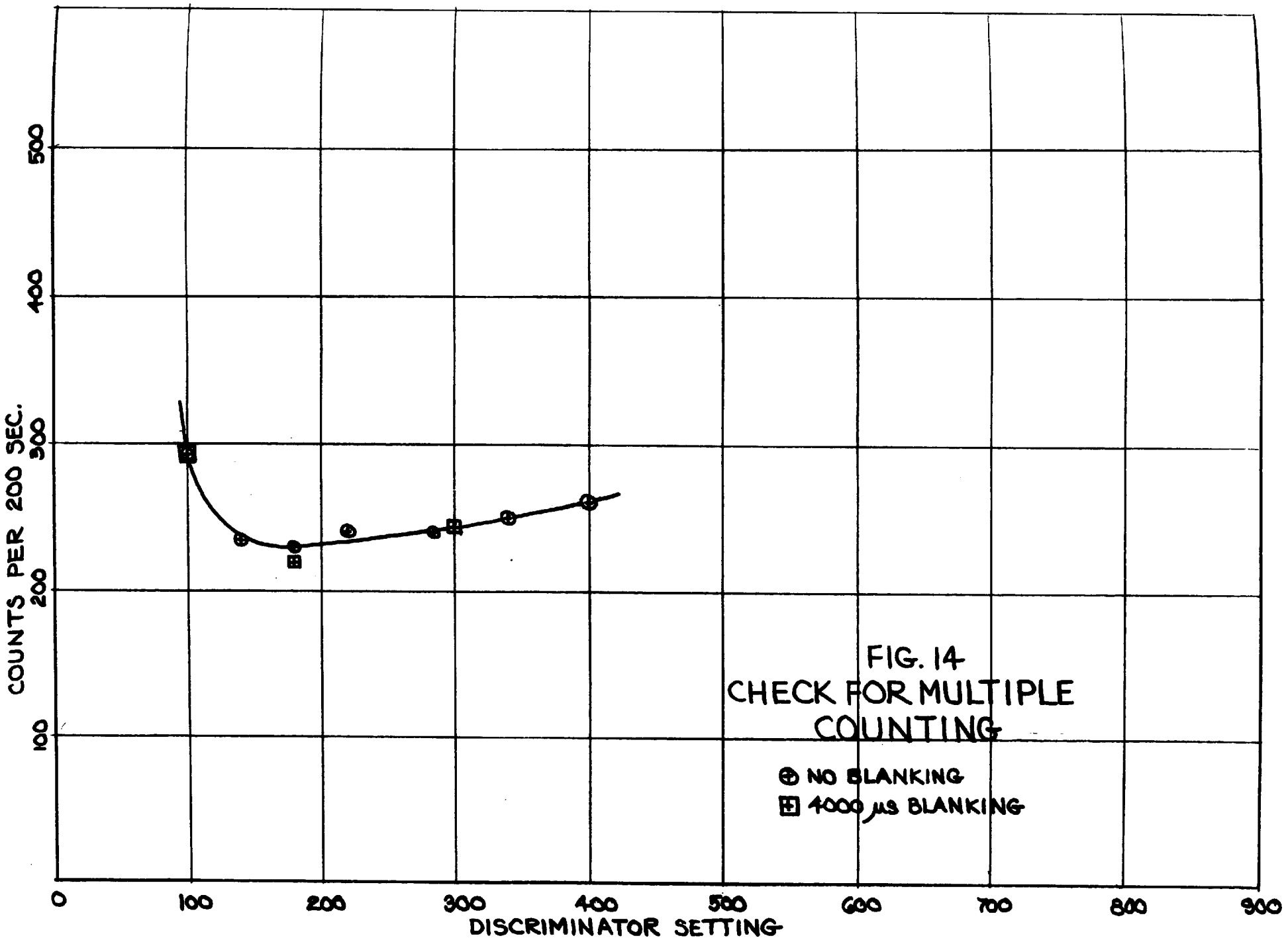


FIG. 14
CHECK FOR MULTIPLE COUNTING

4. CORRECTIONS

The experimental data have to be corrected for four effects:

a) background

b) absorption of the K^{40} 1.46 Mev gamma ray

c) finite resolution of the spectrometer

d) escape of electrons through the crystal surface

a. Background

The background correction was obtained by using the NaI crystal previously described. Considering the relative volumes and densities of the NaI and KI crystals and assuming that the absorption coefficients are quite similar[61] it was estimated that the KI crystal background would be aroung 70% of the measured background with the NaI. At first the K^{40} spectrum was measured using no shielding, but it was later discovered that there was a surprisingly high background at low energies present. Consequently, a second spectrum was obtained using several inches of copper and lead shielding which reduced the background count by a factor of 20. When the corresponding background was used for each run the final spectra were in agreement, thus attesting to the validity of the correction. The background with shielding is included in Fig. 15 which also gives the experimentally observed distribution.

b. Gamma Ray Absorption

In the decay of K^{40} gamma rays are emitted as well as beta particles. Since some of these gamma rays are internally absorbed by the crystal an allowance must be made for their contribution to the observed activity. It would be difficult to calculate this correction in detail and fortunately this is not necessary because it amounts to only a few per cent.

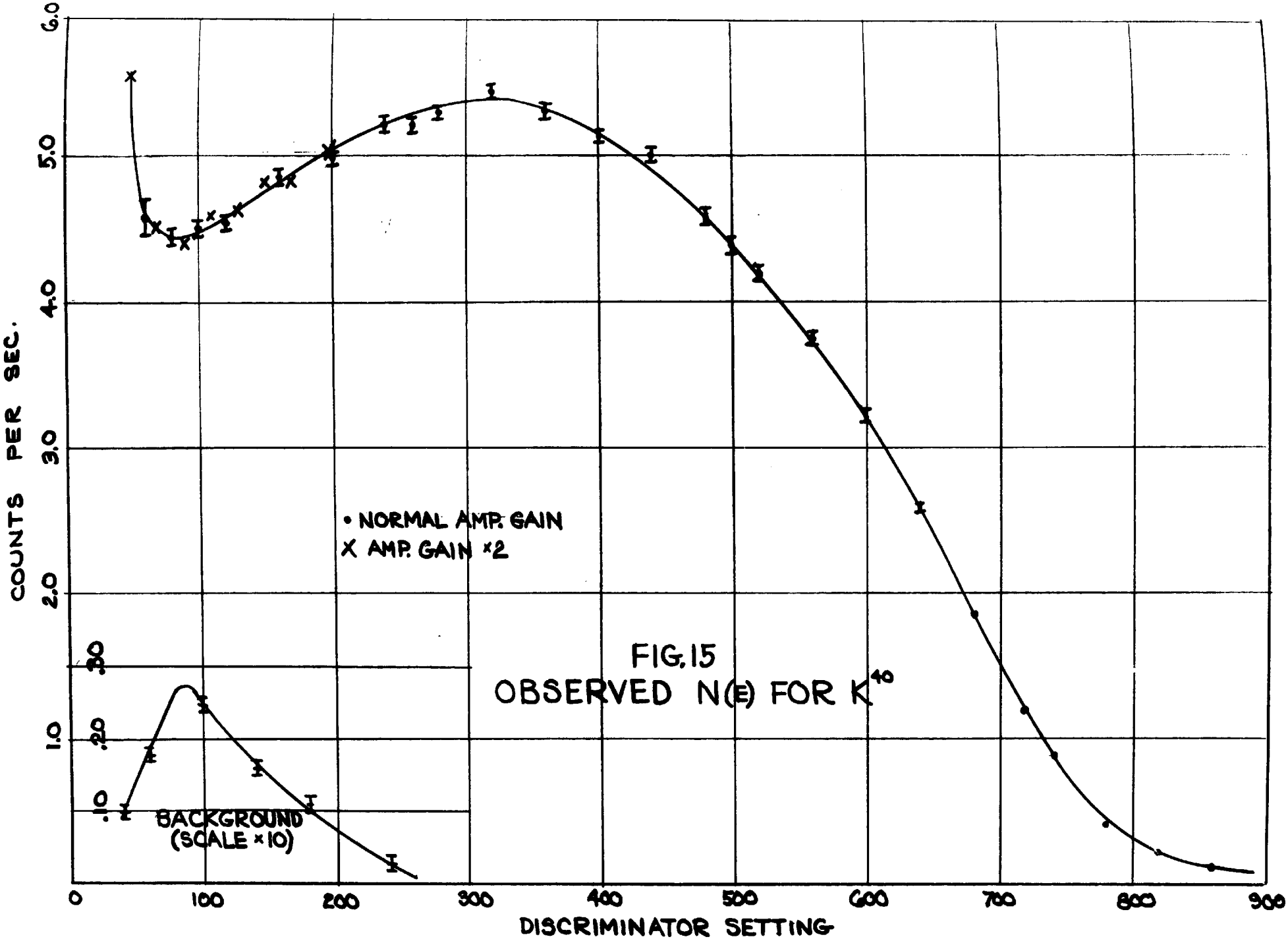


FIG. 15
OBSERVED N(E) FOR K^{40}

By considering the absorption coefficient of KI and the energy[1] and emission rate[62] of the gamma rays, as well as the size and geometry of the crystal, one can readily estimate the gamma ray count to comprise about 2% of the total measured activity. The energy distribution of these counts must also be ascertained. Since a source of gamma rays of around 1.46 Mev was not conveniently available the distribution was estimated using the energy distributions of the gamma rays from Cs^{137}, Zn^{65}, and Na^{22}(1.28 Mev). The values of the main features were plotted against the energy and the curves extrapolated to 1.46 Mev. Then, with a channel width of 25 kev and a total gamma ray count of 4 per second, the distribution of Fig. 16 results and must be subtracted from the observed distribution of Fig. 15.

c. Resolution

The correction for the resolution was calculated using the method of Owen and Primakoff.[63] In their work they assumed that the resolution would have some constant value and that this value could be determined experimentally for a given spectrometer arrangement. However, for the scintillation spectrometer the resolution is not independent of the energy but is proportional to $1/\sqrt{E}$ where the resolution is defined as the ratio of the full width of the peak at half maximum to the energy E of the peak. This dependence of the resolution on the $1/\sqrt{E}$ is what one would expect from statistical considerations of the variations in number of electrons liberated from the photocathode surface by the photons produced upon the absorption of a particle with given energy in the crystal. The experimental values of the resolution at various energies are in agreement.

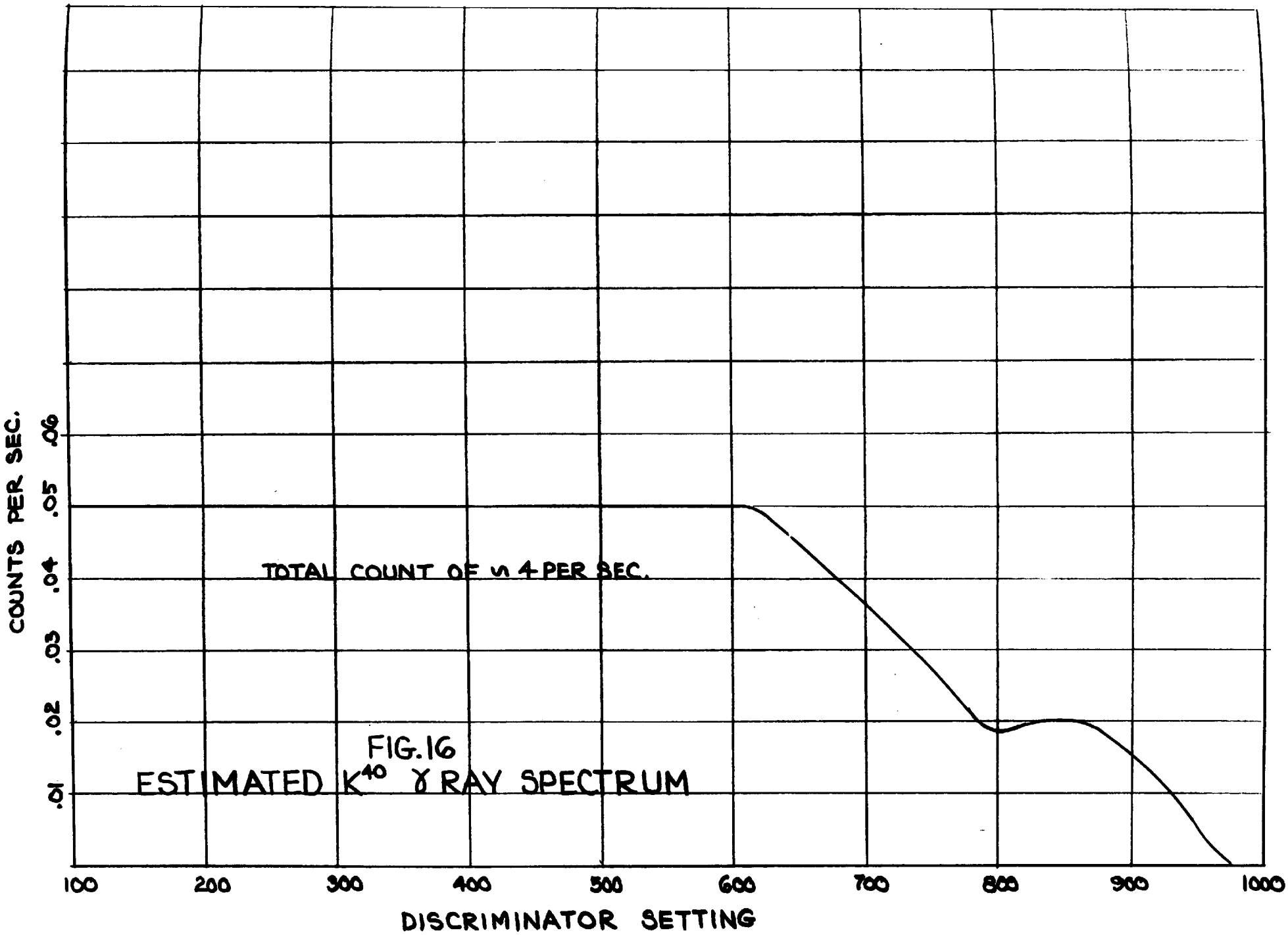


FIG. 16

ESTIMATED K^{40} γ RAY SPECTRUM

If the peaks are assumed to have a gaussian shape then one can write the following relationship between the observed distribution n(E) and the true distribution N(E):

$$n(E) = \int_0^\infty N(E') \frac{\alpha}{\sqrt{\pi E}} e^{-\frac{\alpha^2}{E}(E'-E)^2} dE'$$

This equation can be solved using the Fourier Transform and one gets:

$$N(E) = n(E) - \frac{E}{4\alpha^2} \frac{d^2 n(E)}{dE^2}$$

The value of the constant alpha has to be determined from the observed resolutions. The average of the values from several different peaks gave $\alpha = .29$ when E is in kev. This corresponds to a resolution of about 22% for the Cs^{137} peak at .661 kev. Since the correction term depends on the second derivative and the energy it is small for all points except those at the high energy end of the spectrum where the slope changes rapidly.

d. Surface Effect

Mateosian and Smith[64] have calculated the correction for the escape of electrons from the surface of a crystal using the simplifying assumption "that the path of an individual electron is a straight line in a crystal equal in length to its range, and that the density of light along the path of an electron in a scintillation is constant." However, if one considers electrons of an energy E, the assumption that the path is a straight line equal to the range is not justified. In practice the electron will be scattered many times. Measurements of the absorption of conversion electrons show that the number of electrons

absorbed depends in an approximately linear fashion on the thickness of absorber.[65,66] Consequently, it would be better to assume that the number of electrons traversing a distance ξ in the crystal goes as $(1 - \xi/R)$ where R = the electron range. If this is done one obtains a correction term only half as great as that calculated by Mateosian and Smith.

Since the calculation is carried out the same as theirs, except for the inclusion of the additional factor $(1 - \xi/R)$, only the results will be given here. They are:

1. The fraction of the electrons of energy E which escape from the crystal is equal to 1/8 the volume made by the surface area times the electron range.
2. The energy lost in the crystal by an escaping electron of original energy E has an equal probability of being anywhere in the range from 0 to E.

The range of the electrons was obtained using an empirical range-energy curve[65] for beta particles in Al. A slight adjustment in these values was made since the beta particles were moving in a KI crystal and not in Al. Beta particles lose their energy and are stopped by collisions with the electrons of the absorbing material. Therefore, the stopping power depends on the density of electrons in the absorbing material and is proportional to the Z/A ratio in the absorber. By considering the Z/A ratio for Al and the effective Z/A ratio for the KI crystal one would expect the range in the KI crystal to be about 8% greater than the corresponding range in Al.

Using these results one can make a graphical solution to estimate the correction to be made for each point. First the number of

electrons of original energy E which strike the crystal surface was calculated. This was used as one point on an electron loss versus original energy curve. After enough points had been located, a smooth curve was drawn and used to obtain the electron count lost at the energy of each data point. Next the electron count lost at any one energy was assumed to be divided equally among all the lower energy channels, each channel being 25 kev wide. The total of these contributions from the higher channels was subtracted from the electron loss calculated for that channel at the energy of the data point in question. The net result was added to the value of each point on the experimental beta spectrum. The correction terms were positive in the high energy region and negative in the low energy region of the spectrum.

Table III shows the original data point values, each of the corrections, and the final value for each of the points. The estimated uncertainty is also given for each point. It is obtained by taking the statistical standard deviation and estimating the possible per cent error in each of the correction terms:

Correction term	Per cent error
background	10%
gamma ray	40%
resolution	40%
electron escape	20%

The corrected data points with the estimated errors are plotted in Fig. 17 which is then the true N(E) spectrum for K^{40}.

TABLE III

DATA FOR K^{40}

Discriminator Setting	N(E)	Background	γ Ray	Surface Correction	Resolution Corr.	N(E) net	Error
060	4.58	-.18	-.05	-.18		4.17	±.07
080	4.44	-.27	-.05	-.17		3.95	.06
100	4.51	-.25	-.05	-.16		4.05	.06
120	4.53	-.20	-.05	-.15		4.13	.06
160	4.85	-.13	-.05	-.13		4.54	.06
200	4.98	-.08	-.05	-.10		4.75	.06
240	5.21	-.03	-.05	-.07		5.06	.06
260	5.21		-.05	-.06	.02	5.12	.06
280	5.29		-.05	-.04	.02	5.22	.05
320	5.44		-.05	.00		5.39	.05
360	5.30		-.05	+.03	.05	5.33	.06
400	5.13		-.05	+.06	.04	5.18	.04
440	4.97		-.05	+.09		5.01	.05
480	4.58		-.05	+.11	.03	4.67	.06
520	4.20		-.05	+.12	.03	4.29	.06
560	3.75		-.05	+.13	.02	3.85	.06
600	3.23		-.05	+.13	.04	3.35	.05
640	2.59		-.05	+.12	.04	2.70	.05
680	1.86		-.04	+.08		1.90	.04
720	1.21		-.03	+.07	-.12	1.13	.05
750	.74		-.03	+.03	-.20	.54	.08
780	.41		-.02	+.01	-.24	.16	.10
800	.28		-.02	.00	-.21	.05	.08
820	.21		-.02	.00	-.12	.07	.10

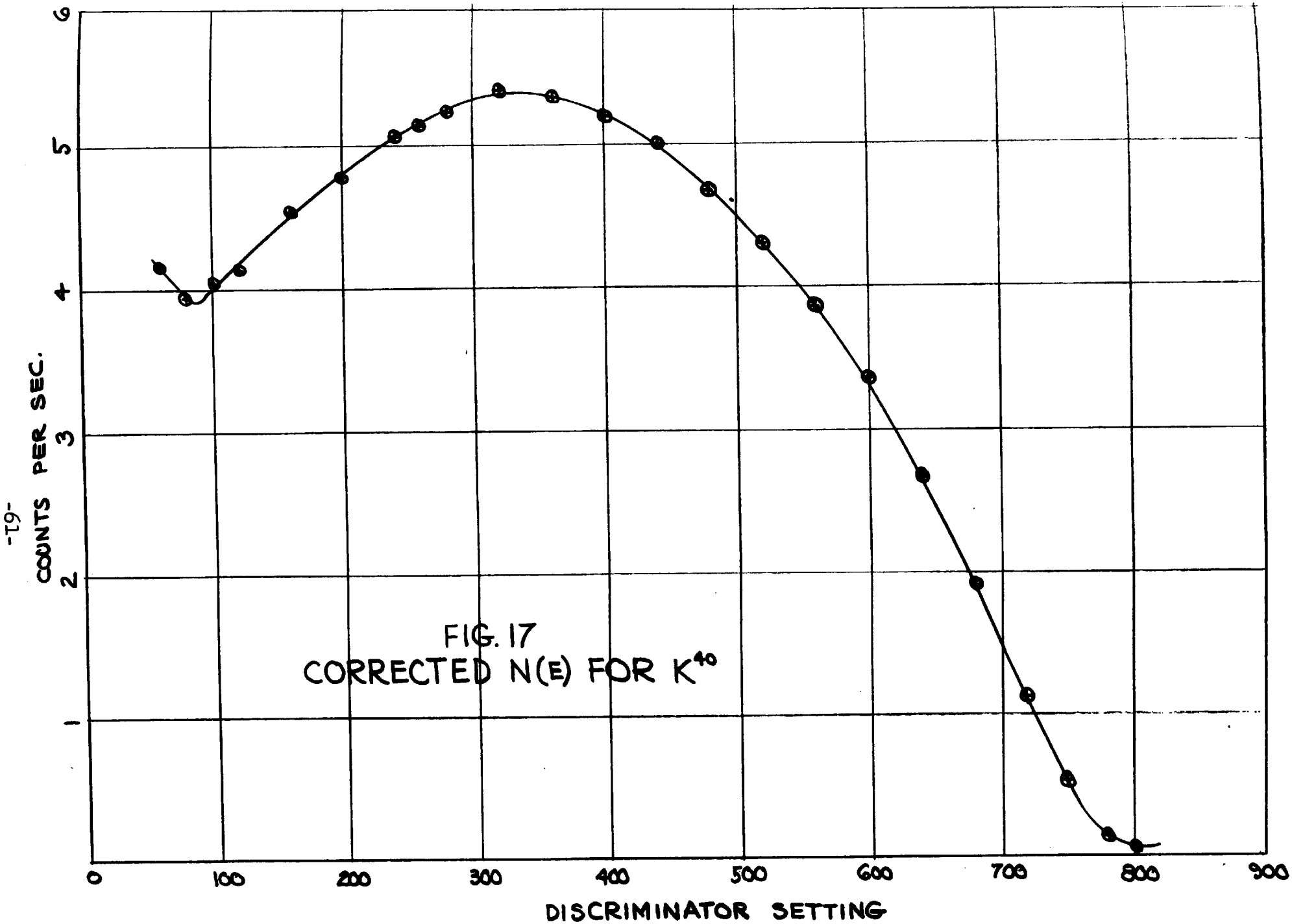


FIG. 17
CORRECTED N(E) FOR K^{40}

5. MEASUREMENT OF THE TOTAL K^{40} BETA ACTIVITY

To measure the total beta activity of the KI crystal the integral count was recorded for various input pulse height settings on the discriminator. As Fig. 18 shows, the resulting integral count curve behaved well down to an energy of about 100 Kev. In this region the curvature changed suddenly. The sudden change was not unexpected as it is in this region that the photomultiplier tube noise becomes noticeable. The data points below 100 Kev were accordingly discarded and the normal curve was extrapolated to zero energy. As can be seen from the figure the activity added by this extrapolation amounted to only about 5% of the total and so the uncertainty in the extrapolation has small effect on the total measured activity. The corresponding background count is also included in the figure and was estimated in the same manner as the background for the differential count.

When the background and total K^{40} gamma ray counts were subtracted an activity of 200 ± 3 counts per second remained. The error was estimated by considering the uncertainties in the extrapolation, background correction and the total gamma ray activity. This value is equivalent to an activity of $27.4 \pm .4$ beta particles per second per gram of natural potassium and agrees well with other measurements using 4π geometry.(57,67)

Taking the relative abundance of K^{40} in natural potassium to be $1.19 \pm .01 \times 10^{-2}$% as determined by Nier(68), the measured activity corresponds to a K^{40} half-life of $1.47 \pm .02 \times 10^{9}$ years. The numbers involved in the calculation are given below.

$$\tau = \frac{.693}{\lambda} \quad \frac{.693 \times 6.023 \times 10^{23} \times 1.19 \times 10^{-4}}{39.01 \times 27.4 \times 3.16 \times 10^{7}} = 1.47 \times 10^{9} \text{ years}$$

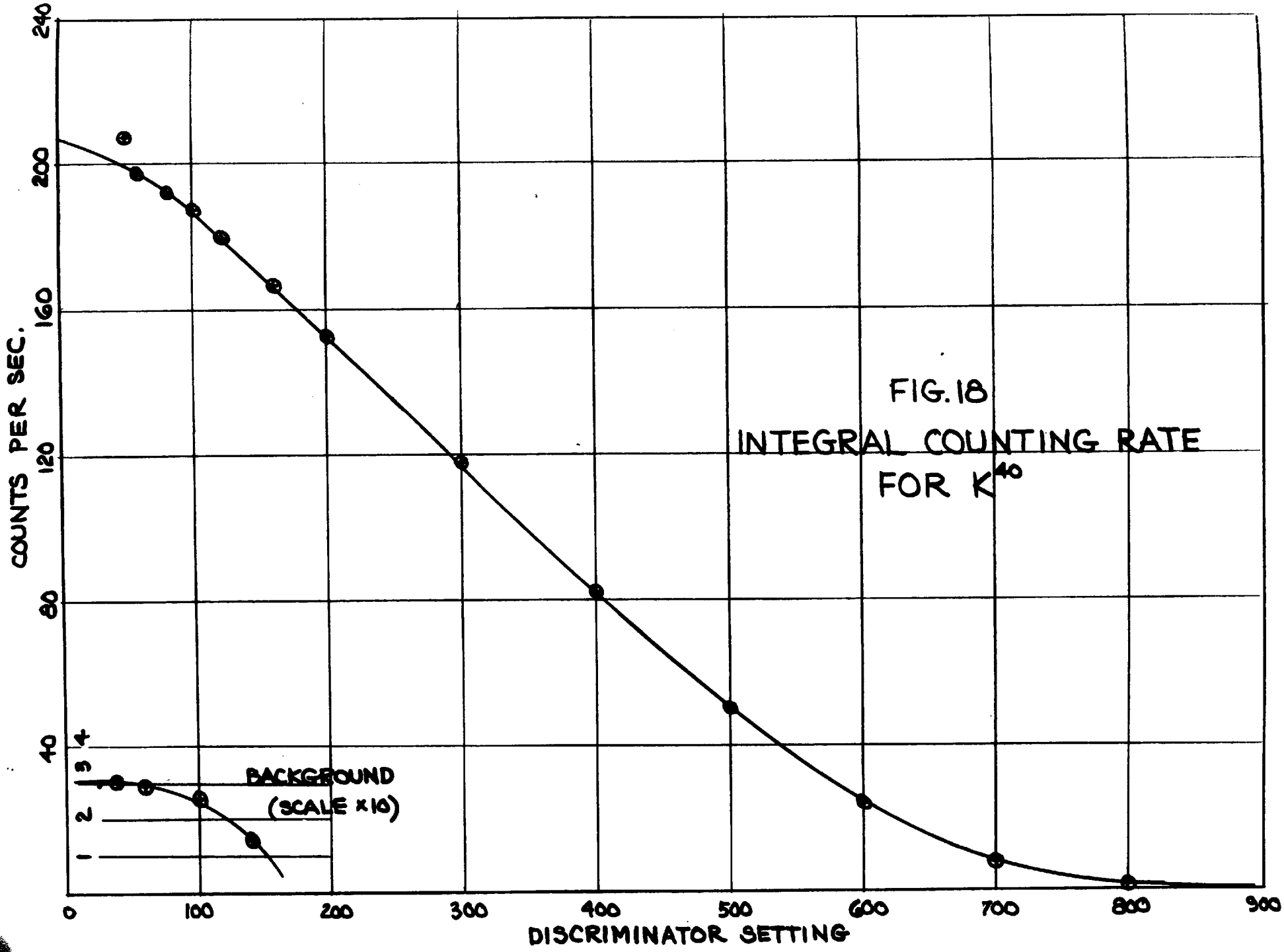


FIG. 18
INTEGRAL COUNTING RATE
FOR K^{40}

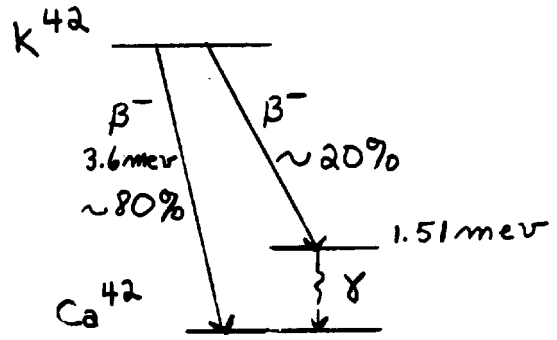
The half-life calculated above is uncorrected for the competing electron capture decay process. If we use Sawyer's[62] result that only 88% of the decaying K^{40} nuclei decay by beta emission then the half-life due to both beta decay and electron capture is 1.29×10^9 years.

6. BETA SPECTRUM OF K^{42}

Another isotope of potassium (K^{42}) also undergoes beta decay and its spectrum should be of the unique first-forbidden type according to Shull and Feenberg[69] who analyzed data taken by Siegbahn[70] and found agreement with the theoretical prediction. Therefore it seemed worthwhile to observe the high energy end of the K^{42} spectrum to see that the scintillation spectrometer gave agreement with the other method as a further check on its reliability.

The radioactive K^{42} was obtained by placing the KI crystal in the neutron flux near the University of Michigan cyclotron. About 8 inches of paraffin wax was placed in front of the crystal so that neutrons reaching the crystal would have low energies. Then, since natural potassium contains about 6.9% K^{41}, a fair K^{42} activity was produced by slow neutron capture when the crystal was irradiated for some 10 hours. An even larger beta activity due to the I^{128} isotope was produced, but since its half-life is 25 minutes as compared to the 14 hour half-life of the K^{42}, the I^{128} activity died away to negligible value in several hours. After that the only activities of any consequence in the crystal were due to the decay of K^{40} and K^{42}.

The decay of K^{42} is complex. Its decay scheme is as follows:[1]



From the decay scheme one can see that a measurement of beta particles emitted with an energy above 2 Mev should give the high energy end of the 3.6 Mev beta spectrum and it is this spectrum which has been predicted to be of the unique first-forbidden type.

The spectrum of the beta particles with energies above 2 Mev was obtained and corrected for the resolution and electron escape through the surface as already described for the K^{40} spectrum. In this energy region the background is negligible and no correction is necessary for the self-absorption of gamma rays.

CHAPTER V

THEORY OF BETA DECAY

The present theory of beta decay was introduced by Fermi in 1934.[71] Since that time many authors have discussed and extended the original theory in detail, covering all phases of the problem of beta decay.

In general there are three types of beta decay:

electron emission (β^-) $N \rightarrow P + \beta^- + \bar{\nu}$

positron emission (β^+) $P \rightarrow N + \beta^+ + \nu$

orbital electron capture $P + e^- \rightarrow N + \nu$

N = neutron, P = proton, ν = neutrino, and $\bar{\nu}$ = antineutrino. In this thesis only a summary will be given of that part of the theory pertinent to the β^- decay of K^{40} along with a discussion of the agreement between the experimental results and the theoretical predictions.

Fermi proposed a theory analogous to the Dirac theory of the emission of light using Pauli's neutrino hypothesis that, during beta decay, an additional particle called a neutrino is emitted with the beta particle and that the neutrino and beta particle between them carry away the energy released during the nuclear transition. There are two possible descriptions of the nature of the neutrino. One, in analogy to the Dirac electron-positron theory, assumes that there should be distinguishable neutrino and antineutrino particles. The other is a proposal by Majorana[72] that all neutrinos are indistinguishable. It

is extremely difficult to verify the validity of either assumption experimentally. At present the indirect experimental evidence obtained from double beta decay processes seems to favor the neutrino-antineutrino picture.

The general expression for the decay rate can be written in the form:

$$d\lambda = \frac{2\pi}{\hbar} |H_{if}|^2 \rho(E) = \text{number of transitions per sec.}$$

where: $\rho(E)$ = the number of final states per unit range of energy release,

H_{if} = the transition matrix element.

For β^- decay the final states are assumed to be characterized by electrons of total energy E_e and momentum p and by neutrinos of total energy E_ν and momentum q where in each case conservation of energy is maintained. (i.e., $E_0 = E_e + E_\nu$ = total disintegration energy.) Then if one further assumes that all possible divisions of the energy are equally probable, $\rho(E)$ can be written as follows:[73]

$$\rho(E_0) = \frac{V^2}{4\pi^4 \hbar^6 c^3} p_e^2 (E_0 - E_e)^2 dp_e$$

or

$$P(E_e)dE_e = C' E_e p_e (E_0 - E_e)^2 dE_e$$

$P(E_e)$ = energy distribution of the emitted electrons due to the "statistical" factor.

and

$$d\lambda = C |H_{if}|^2 E_e p (E_0 - E_e)^2 dE_e$$

V = volume of an imaginary box inclosing the system and has merely a formal significance in the calculation,

$$C' = \frac{V^2}{2\pi^3 \hbar^7 c^5} = \text{a constant}$$

$$C = \frac{2\pi}{\hbar} C'$$

The H_{if} matrix element contains the wave functions of the four particles involved in the interaction.

$$H_{if} = \sum_n \int F(r_n) \, (\phi_f^* \, K_n \phi_i) \, d\tau$$

where $F(r_n)$ depends on the wave functions of the electron and neutrino at the position of the n^{th} nucleon in the nucleus which is the one considered to be undergoing beta decay.

ϕ_i and ϕ_f are the wave functions of the initial and final states of the nucleus and K_n is an operator connected with the beta decay of the n^{th} nucleon. It can change the n^{th} nucleon from a proton into a neutron or vice versa.

F can be written in the bilinear form:

$$F(r_n) = \left\{ \phi_e^* (r_n), \; \Delta \, \phi_\nu^* (r_n) \right\}$$

provided the operator Δ does not contain any derivatives, an assumption made for reasons of simplicity but which appears to be borne out by experiment. The operator Δ in this case is a 4 x 4 matrix. The complex conjugates of the neutrino and electron wave functions are used because they belong to the final state of the system and one always takes the complex conjugate of the final state so that the square of the matrix element will yield a real number for the probability.

If the effect of the coulomb field on the electron is neglected we can consider the space part of the neutrino and electron wave

functions as being plane waves and put

$$\phi_e(r) = V^{-1/2} U_e e^{\frac{i}{\hbar} p \cdot r} = \text{electron wave function}$$

$$\phi_\nu(r) = V^{-1/2} U_\nu e^{\frac{i}{\hbar} q \cdot r} = \text{neutrino wave function}$$

where U_e is the Dirac spinor wave function with four components for the electron and U_ν is similarly defined for the neutrino.

In general the effect of the coulomb field on the electron is not negligible and so one must include a factor of $\left[F(Z,E)\right]^{1/2}$ in the matrix element to account for this effect. $F(Z,E)$ is difficult to calculate explicitly, but various approximate expressions have been derived[73] and tables are now available.[74] Non-relativistically one can consider

$$F(z,E) = \frac{\left|\phi_e(0)\right|^2}{\left|\phi_e(0)\right|^2_{\text{free}}}$$

When these quantities are substituted for F we see that

$$H_{if} \sim \left[F(Z,E)\right]^{1/2} e^{-\frac{i}{\hbar}(p+q)\cdot r}$$

For all practical cases p and q are so small that as long as r is of nuclear dimensions the quantity $(p+q)\cdot r/\hbar \approx 1/10$ and an expansion of the exponential term is feasible. For any given transition matrix element one then has a series of terms of decreasing magnitude. Only the first term for which the matrix element has a non-vanishing value is of importance in the transition. The value of the exponent ℓ in each of the series terms designates the order of the transition as well as determining the orbital angular momentum carried away by the beta particle and the neutrino. In an allowed transition $\ell = 0$, while for the third-forbidden transition predicted for K^{40} $\ell = 3$.

So far nothing has been said about the type of interaction term necessary in the matrix element to describe a beta transition. Since we are dealing with a phenomenon of nature, it seems reasonable to require that the transformation matrix be invariant under rotations, inversions, and proper Lorentz transformations. If this is done then the number of permissible choices for the interaction having the proper form is sharply curtailed. Pauli[75] has shown that there can be only five different expressions, each with an appropriate choice of A and the corresponding K_n. The five interactions are named; scalar, vector, tensor, axial vector, and pseudoscalar. Each name is a consequence of the nature of the integrand in the equation for H_{if}. For instance, the vector interaction has an integrand that consists of the scalar product of two four-vectors. Since the detailed expressions for these interactions are readily available[73] and are not of importance in this discussion, they are not given here.

To sum up the results so far we may say that the decay rate can be expressed as follows:

$$d\lambda = C\left|M\, e^{-\frac{i}{\hbar}(p+q)\cdot r}\right|^2 F(Z,E)(E_e-1)^{1/2}(E_0-E_e)^2 dE_e$$

where M can be the matrix element of any of the five interactions (after the substitution of plane waves for the space parts of ϕ_e and ϕ_ν) or any linear combination of them. Since the proper choice of M cannot be obtained from the theory one must use the results of experiment for its determination. Recent experimental evidence indicates quite clearly that the correct beta coupling must be some linear combination of the scalar and tensor interactions.

1. SELECTION RULES

Depending on the choice of M there are certain selection rules which must be obeyed for any given transition in order to have a non-vanishing matrix element. There are two kinds of these selection rules; Fermi selection rules which characterize transitions with scalar and vector interactions, and Gamow-Teller rules characterizing transitions with tensor and axial vector interactions. In any given order the spin changes (ΔI) permitted by the Gamow-Teller rules are one unit greater than those permitted by the Fermi selection rules. Thus for allowed ($\ell = 0$) transitions $\Delta I=0$ under Fermi rules and $\Delta I = 0 \pm 1$ (not $0 \rightarrow 0$) under the Gamow-Teller rules with no parity change in either case.

2. SHAPE OF THE BETA SPECTRUM

Letting $N(E)$ be the number of electrons emitted per unit energy range one gets the energy spectrum of the emitted beta particles of energy E

$$N(E)dE = C\left|Me^{-\frac{i}{\hbar}(p+q)\cdot r}\right|^2 F(Z,E)(E^2-1)^{1/2}(E_0-E)^2dE$$

If one now considers allowed transitions where $e^{-\frac{i}{\hbar}(p+q)\cdot r} = 1$ and $|M|^2$ = a constant then:

$$N(E)dE = CG^2F(Z,E)(E^2-1)^{1/2}(E_0-E)^2dE$$

G = the interaction strength constant.

By plotting $\left[N(E)/F(Z,E)(E^2-1)^{1/2}\right]^{1/2}$ against E a straight line results which intersects the abscissa at $E = E_0$. This called either a "Kurie" or "Fermi" plot.

For the unallowed ($\ell \neq 0$) transitions a shape correction factor must be included because of the presence of the n^{th} term in the expansion of the exponential.

In the general case more than one matrix element can make an appreciable contribution to the transition, but the discussion here will be limited to the unique forbidden transitions. They correspond to the physical situation in which the electron and neutrino are emitted with their spins in the same direction and also parallel to the orbital angular momentum. In this case $|\Delta I| = \ell + 1$ with the Gamow-Teller selection rules applying so that the interaction type can be either tensor or axial vector or both. The dominant contribution comes from only one nuclear matrix element and the n^{th} term gives a probability proportional to $|p+q|^{2n}$. When this is averaged over all directions of the electron and neutrino momenta, p and q, one obtains the shape correction factor:(76)

$$a_n(E) = \sum_{i=0}^{n} \frac{(2n+1)!\, p^{2i} q^{2(n-i)}}{(2i+1)!(2n-2i+1)!} \qquad (7)$$

The shape correction factor can be used along with usual non-relativistic expressions for $F(Z,E)$ to give a good relativistic approximation as long as $Z/137 \ll 1$. It should also perhaps be noted that the factor favors those transitions in which either the electron or the neutrino gets most of the available energy.

Then if one plots

$$\left[\frac{N(E)}{a_n(E)F(Z,E)(E^2-1)^{1/2}E}\right]^{1/2} \quad \text{against } E$$

a straight line should also be obtained for unique forbidden transitions.

CHAPTER VI

APPLICATION OF THEORY TO EXPERIMENTAL RESULTS

1. FERMI PLOT OF K^{40}

As was mentioned earlier the K^{40} nucleus has been found to have a spin of 4. Using the shell theory its parity is predicted to be odd.(77) The daughter nucleus Ca^{40}, being an even-even nucleus, should have zero spin and an even parity.(43) Under these conditions the transition should be of the unique third-forbidden type(51,52) and the allowed Fermi plot non-linear. Figure 19 shows the allowed Fermi plot for K^{40} and it is non-linear. From Eq.(7) which gives the shape correction factors we see that for $n = 3$:

$$a_3 = p^6 + 7p^4q^2 + 7p^2q^4 + q^6$$

Applying this correction factor a straight line plot is obtained down to about 200 kev. (See Fig. 19). This indicates that the measured spectrum agrees with the theoretical predictions. However, as pointed out by Alburger(54), it is difficult to distinguish between the effects of using either the unique second or third-forbidden correction factors and as a test n was chosen = 2 also.

$$a_2 = p^4 + 10/3\ p^2q^2 + q^4$$

When a_2 was applied to the spectrum an equally good linear Fermi plot resulted which appears linear down to an energy of around 200 kev.

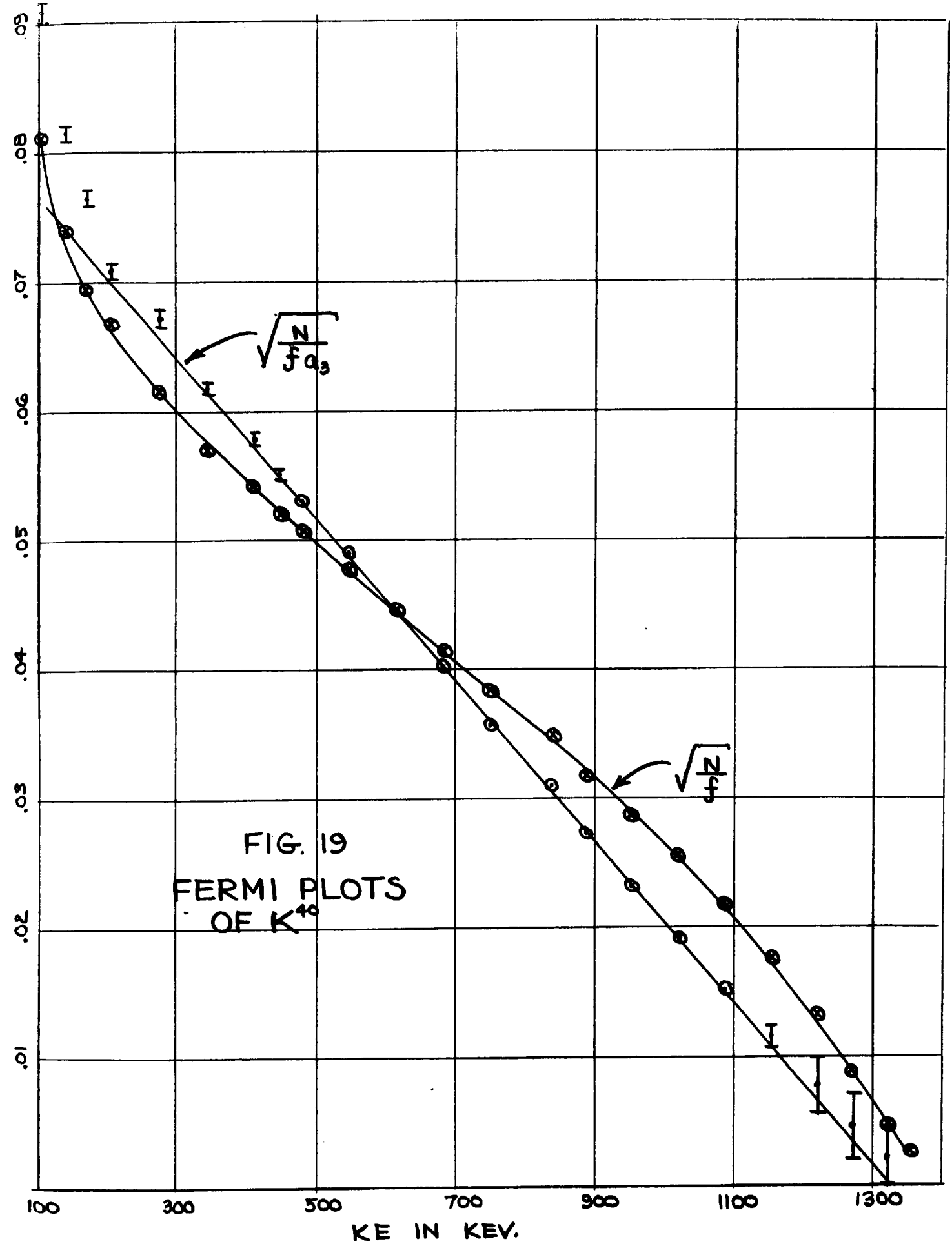


FIG. 19
FERMI PLOTS
OF K^{40}

(See Fig. 20.) For a further test the unique first-forbidden correction factor ($a_1 = p^2 + q^2$) was applied. The Fermi plot is also shown in Fig. 20. The maximum beta energies taken from the second and third-forbidden Fermi plots differ by about 1-1/2%. Using the a_3 correction factor $E_0 = 1.33$ Mev while the a_2 factor gives $E_0 = 1.35$ Mev. If one assumes that a_3 is really the correct factor to be employed in accord with the theory then $E_0 = 1.33 \pm .01$ Mev. This value agrees well with the results of Feldman and Wu[55], but is slightly higher than the maximum energy obtained by Good.[57]

On all of the curves the flags indicate the total uncertainty in the points. From the figure one can see that the first-forbidden factor causes a definite deviation from linearity at higher energies than the first two. Thus one can say that the experimentally observed shape definitely favors a unique second or third-forbidden transition, but does not distinguish between the two. In order to do this some method must be obtained for observing the low energy region of the spectrum in greater detail.

2. FERMI PLOT OF K^{42}

Figure 21 shows the allowed Fermi plot of the observed K^{42} β^- spectrum in the energy region from 2 to 3.6 Mev together with the results of applying the unique first-forbidden correction factor. The allowed plot is non-linear while the corrected plot is linear. Since this is in good agreement with the work of Shull and Feenberg[67], it it adds evidence for the reliability of the method used to determine the K^{40} spectrum. The fact that the maximum beta energy of 3.73 Mev was about 3% higher than previous results is not regarded as being particularly significant because there was a few per cent uncertainty in the

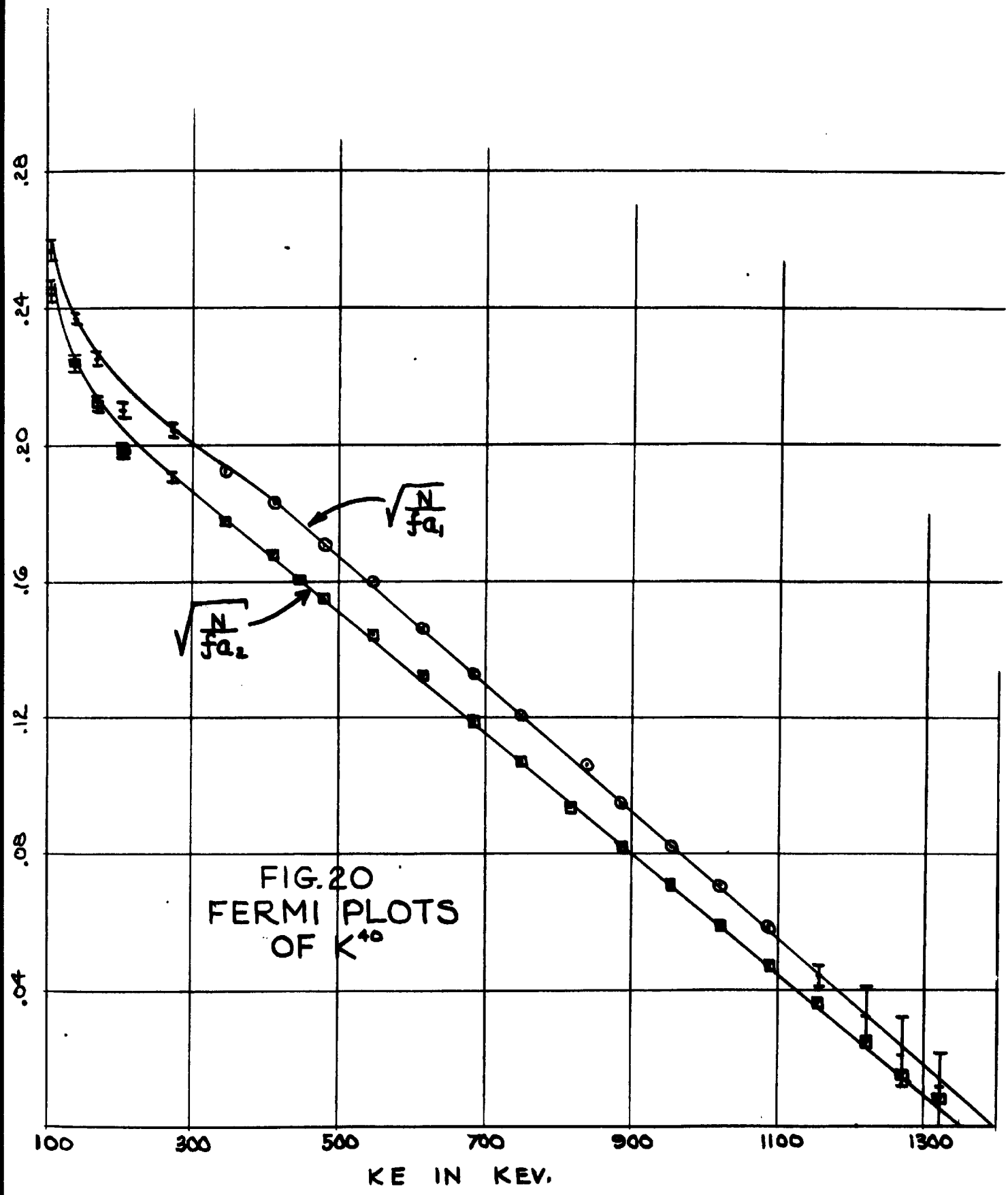


FIG. 20
FERMI PLOTS
OF K^{40}

energy calibration during the measurement.

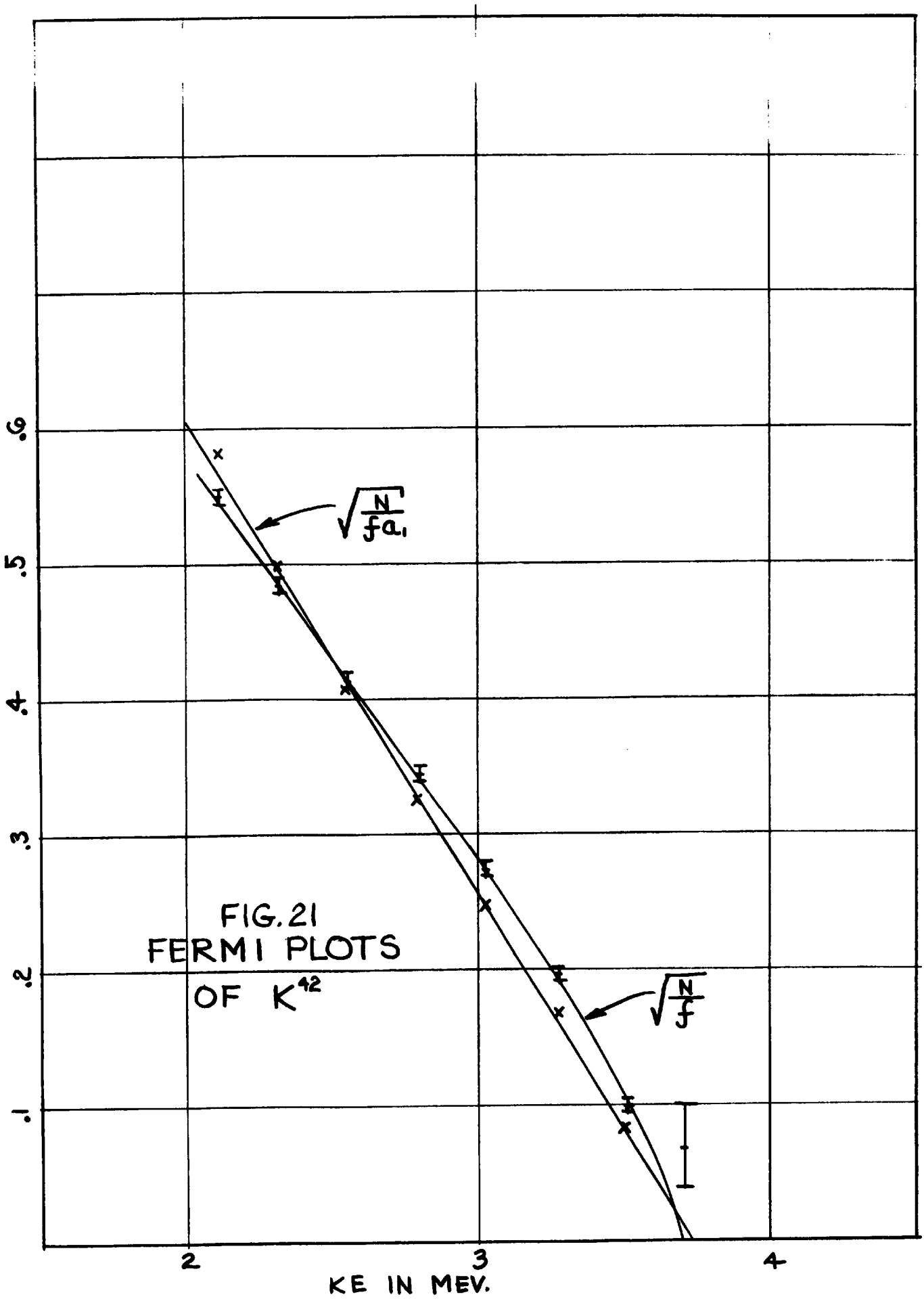


FIG. 21
FERMI PLOTS
OF K^{42}

REFERENCES

1. Hollander, Perlman, and Seaborg, Rev. Mod. Phys. 25, 469, (1953) (Table of Isotopes)
2. M.H. MacGregor and M.L. Wiedenbeck, Phys. Rev. 94, 138 (1954)
3. Waldron, Schultz, and Kohman, Phys. Rev. 93, 254 (1954)
4. W. Porschen and W. Piezler, Z. Naturforsch 8a, 502 (1953)
5. G. Hevesy and M. Pahl, Nature 130, 846 (1932)
6. B. Weaver, Phys. Rev. 80, 301 (1950)
7. Rasmussen, Reynolds, Thompson, and Ghiorso, Phys. Rev. 80, 475 (1950)
8. Hevesy, Pahl, and Hosemann, Z. Physik 83, 43 (1933)
9. W.F. Libby, Phys. Rev. 46, 196 (1934)
10. R. Hosemann, Z. Physik 99, 405 (1936)
11. H.F. Taylor and V.D. Dabholker, Phys. Soc. Proc. 48, 285 (1936)
12. M. Mäder, Z. Physik 88, 601 (1934)
13. E. Picciotto, Compt rend, Paris, 229, 117 (1949)
14. C.M.G. Lattes and P. Cuer, Nature 158, 197 (1946)
15. Inghram, Hess, and Hayden, Phys. Rev. 73, 180 (1948)
16. Fairmount Chemical Company (private communication)
17. Obtained from the Carbide and Carbon Chemicals Company, Oak Ridge, Tenn.
18. G.A. Sawyer, thesis, University of Michigan (1950)
19. L.L. Quill, Nuclear Energy Series IV 19B , McGraw-Hill Book Company, Inc., New York, 125,219 (1950)
20. Yost, Russell, and Garner, The Rare Earth Elements and Their Compounds, John Wiley and Sons, Inc., New York, Chapter 6 (1947)
21. M.I.T. Wavelength Tables ed. by G.R. Harrison, John Wiley and Sons, Inc., New York, 291 (1939)
22. W.A. Higgenbotham, Rev. Sci. Instr. 22, 429 (1951)

23. W.C. Elmore and M. Sands, Electronics: Experimental Techniques, McGraw-Hill Book Company, Inc., 235 (1949)

24. Y. Beers, Theory of Error, Addison-Wesley Publishing Company, Inc., 38 (1953)

25. H. Yagoda, Radioactive Measurements with Nuclear Emulsions, John Wiley and Sons, Inc., New York, 257 (1949)

26. A. Beiser, Rev. Mod. Phys. 24, 273 (1952)

27. K.K. Keller and K.B. Mather, Phys. Rev. 74, 624 (1948)

28. F. Bestenreiner and E. Broda, Nature, 164, 658 (1949)

29. Haenny, Najar, and Gailloud, Helv. Phys. Acta 22, (No. 6) 611 (1949)

30. D. Stzeinsznaider, J. Phys. et Radium 14, 465 (1953)

31. W.P. Jesse and J. Sadauskis, Phys. Rev. 78, 1 (1950)

32. G.C. Hanna, Phys. Rev. 80, 530 (1950)

33. Rhodes, Franzen, and Stephens, Phys. Rev. 87, 141 (1952)

34. P.R. Tunnicliffe and G.A. Ward, Proc. Phys. Soc. 65, 233 (1952)

35. T.E. Cranshaw and J.A. Harvey, Canadian J. Res. 26A, 243 (1948)

36. E. Fermi, Nuclear Physics, (Notes compiled by Orear et al) The University of Chicago Press, 7 (1950)

37. T.P. Kohman, Phys. Rev. 76, 448 (1949)

38. M.G. Mayer, Phys. Rev. 75, 1969 (1949)

39. D.C. Dunlavey and G.T. Seaborg, Phys. Rev. 92, 206 (1953)

40. G. Gamow, Z. Physik 52, 510 (1929)

41. E.U. Condon and R.W. Gurney, Phys. Rev. 33, 127 (1929)

42. J.M. Blatt and V.F. Weiskopf, Theoretical Nuclear Physics, John Wiley and Sons, Inc., 783 (1952)

43. ibid. Chapter XI

44. H.A. Bethe, Rev. Mod. Phys. 9, 161 (1937)

45. Rasmussen, Thompson, and Ghiorso, Phys. Rev. 89, 33 (1953)

46. S. Biswas and A.P. Patro, Indian J. Phys. 22, 540 (1948)

47. I. Perlman and T.J. Ypsilantis, Phys. Rev. 79, 30 (1950)

48. N.F. Ramsey, Nuclear Moments, John Wiley and Sons, Inc., New York, 84 (1953)

49. G.S. Bogle and H.E.D. Scovil, Proc. Phys. Soc. 65A, 368 (1952)

50. J.R. Zacharias, Phys. Rev. 60, 168 (1941)

51. R.E. Marshak, Phys. Rev. 70, 980 (1946)

52. E. Greuling, Phys. Rev. 61, 568 (1942)

53. D.E. Alburger, Phys. Rev. 75, 1442 (1949)

54. D.E. Alburger, Phys. Rev. 78, 629 (1950)

55. L. Feldman and C.S. Wu, Phys. Rev. 76, 698 (1949)

56. Bell, Weaver, and Cassidy, Phys. Rev. 77, 399 (1950)

57. M.L. Good, Phys. Rev. 83, 1054 (1951)

58. J.H. Marshall, Phys. Rev. 91, 905 (1953)

59. C.W. Johnstone, Nucleonics V. 11 No. 1, 36 (1953)

60. D.C. Lu, Thesis, University of Michigan (1954)

61. J.B Birks, Scintillation Counters, McGraw-Hill Book Company, Inc., 53,55 (1953)

62. G.A. Sawyer and M.L. Wiedenbeck, Phys. Rev. 76, 1535 (1949)

63. G E. Owen and H. Primakoff, Phys. Rev. 74, 1406 (1948)

64. E. der Matesoian and A. Smith, Phys. Rev. 88, 1186 (1952)

65. L.E Glendenin, Nucleonics, V. 2 No. 1, 12 (1948)

66. Rutherford, Chadwick, and Ellis, Radiations from Radioactive Substances, Cambridge University Press, London, 411 (1930)

67. G.A. Sawyer and M.L. Wiedenbeck, Phys. Rev. 79, 490 (1950)

68. A.O. Nier, Phys. Rev. 77, 789 (1950)

69. F.B. Shull and E. Feenberg, Phys. Rev. 75, 1768 (1949)

70. K. Siegbahn, Arkiv. f. Mat., Astr. o. Fys. 34B, No. 4 (1946)

71. E. Fermi, Z. Physik, 88, 161 (1934)

72. E. Majorana, Nuovo Cimento 14, 171 (1937)

73. J.M. Blatt and V.F. Weiskopf, Theoretical Nuclear Physics, John Wiley and Sons, Inc., New York, Chapter XIII (1952)

74. Tables for the Analysis of Beta Spectra, National Bureau of Standards, U.S. Government Printing Office, Washington (1952)

75. W. Pauli, Ann. Inst. Henre Poincare 6, 109 (1936)

76. E.J. Konopinski and L.M. Langer, Annual Review of Nuclear Science 2 301 (1953)

77. E. Feenberg and K.C. Hammack, Phys. Rev. 75, 1877 (1949)